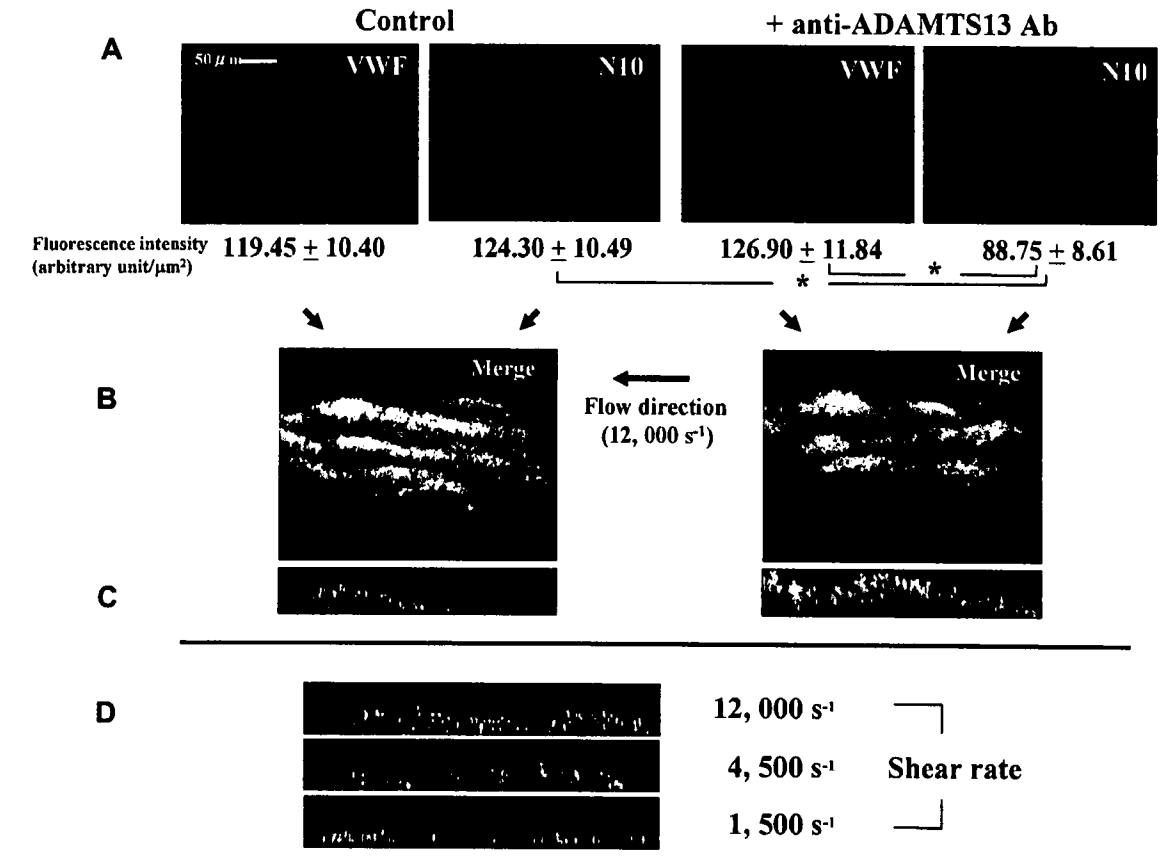


**Figure 2. Visual evaluation of ADAMTS13 activity within thrombi generated under high shear rate conditions using a monoclonal antibody (N10) that specifically detects ADAMTS13-cleaved VWF.** Experimental conditions were as described in Figure 1, except that platelets were not labeled. Thrombi generated on a collagen-coated glass surface at 3 minutes' perfusion with or without an anti-ADAMTS13 antibody under 12 000 $s^{-1}$ shear were fixed, reacted with both N10 antibody and anti–whole VWF antibody, double-stained with Cy3 (red)- and FITC (green)-fluorescence, and viewed by CLSM. (A) Three-dimensional images of thrombi, representative of 5 independent flow experiments, and the corresponding fluorescence intensity (mean ± SD of 5 areas randomly selected in a single perfusion) corrected for background value (negative control IgGs), indicate that VWF cleavage by ADAMTS13 (red color) within thrombi is significantly (*; $P < .01$) reduced in the presence of anti-ADAMTS13 antibody as compared with control thrombi (original magnification; ×600). (B) Merged 3-dimensional images and (C) the corresponding longitudinal views of thrombi; in the merged images, portions stained with both green and red fluorescence basically show the color of the higher pixel value, whereas a yellowish color is seen when both pixel values are nearly equal. Thus, the predominantly reddish appearance of the surface portions of control thrombi suggests that ADAMTS13 is more active on the surface of thrombi forming under very high shear rate conditions, while this tendency is barely visible in the presence of anti-ADAMTS13 antibody. (D) Longitudinal views of thrombi, generated at 3 minutes' perfusion without an anti-ADAMTS13 antibody under various shear rates and double-stained, are representative of 5 separate experiments. Note the prominent red color, especially at the surface portions of thrombi, indicating higher ADAMTS13 activity under higher shear rates.

Under a very high shear rate of 12 000 $s^{-1}$, thrombus growth was significantly accelerated by addition of anti-ADAMTS13 antibody (Figure 1). This enhanced thrombogenesis most likely reflects a block in ADAMTS13 activity rather than nonspecific effects of antibody on platelets, since immunostaining of thrombi with N10 antibody, which reacts only with VWF cleaved by ADAMTS13, visually confirmed the reduced VWF cleavage within thrombi by the anti-ADAMTS13 antibody (Figure 2A). Thus, these results clearly point to the regulatory role of ADAMTS13 during thrombus generation.

While the preceding observations were made under a much higher shear rate than the high shear rate typically used in platelet functional studies (ie, 1500 $s^{-1}$ in our laboratory[14-16]), similar observations, although less pronounced, were confirmed under lower shear rates (Figure 2D). In addition, longitudinal views of thrombi revealed the preferential VWF-cleavage activity of ADAMTS13 at the surface portions of forming thrombi during thrombogenesis (Figure 2B,C). The thrombus surface is thought to directly encounter blood flow with the highest shear rate under such flow circumstances, where the wall shear rate can increase as the flow path narrows in parallel with thrombus growth.[15] Together, these observations strongly suggest a shear rate–dependent property of ADAMTS13 function.

Shear forces are thought to transform the globular conformation of the immobilized VWF multimer observed under static conditions to a shape resembling a spreading bird wing, consistent with the shear rate–dependent acceleration of the VWF-glycoprotein Ib interaction under high shear.[18] By analogy, a stretching of the VWF multimeric structure by shear forces may also be critical for the action of ADAMTS13 in exposing the latent reactive site on the VWF molecule. In this regard, increased tensile strength of the VWF multimeric structure on binding to platelets might augment the stretching effects of shearing forces, resulting in up-regulated ADAMTS13 activity.[19,20] This possibility seems compatible with recent findings indicating that even under low shear rate conditions, ADAMTS13 can cleave ULVWF released from endothelial cells,[9,10] because a greater number of platelets can bind spontaneously to ULVWF as compared with normal-sized VWF without shearing forces.

The mechanisms described here represent an exquisite orchestration by platelets, VWF, and ADAMTS13 under high shear to properly regulate the final size of mural thrombi in vivo and

prevent excessive thrombogenesis from occluding the vessel lumen. Because ADAMTS13 activity appears to be triggered in response to the increased local shear rate associated with the development of thrombi, our results may provide a novel avenue toward strategies that prevent arterial thrombosis without bleeding complications.

## Acknowledgments

We thank Marina Hoffman for editorial assistance.

This work was supported in part by Ministry of Education, Culture, Sports, Science and Technology of Japan grants 15390305 and 19591129 (M.S.), 19592095 (K.N.), and 17390304 (A.Y.), and by the Ministry of Health and Welfare of Japan (M.S.) for Clinical Research of Myocardial Infarction, Stroke and Diabetes Mellitus.

## Authorship

Contribution: Y.S. performed most of the flow experiments, data analysis, and the manuscript preparation; T.M. and M.H. helped perform the flow experiments and data analysis; S.K., M.M., and Y.F. produced and characterized monoclonal antibodies; A.Y. and K.O. provided direction throughout the work and helped prepare the manuscript; and M.S. and K.N. provided the overall experimental designs and direction of this work, and prepared the manuscript.

Conflict-of-interest disclosure: The authors declare no competing financial interests.

Correspondence: Mitsuhiko Sugimoto, MD, or Kenji Nishio Department of Pediatrics, Nara Medical University, 840 Shijo-cho, Kashihara, Nara 634-8522, Japan; e-mail: sugi-ped@naramed-u.ac.jp. or knishio@naramed-u.ac.jp.

## References

1. Sadler JE. von Willebrand factor: two sides of a coin. J Thromb Haemost. 2005;3:1702-1709.
2. Tsai HM. Shear stress and von Willebrand factor in health and disease. Semin Thromb Hemost. 2003;29:479-488.
3. Furlan M. Deficient activity of von Willebrand factor-cleaving protease in thrombotic thrombocytopenic purpura. Expert Rev Cardiovasc Ther. 2003;1:243-255.
4. Lammle B, George JN. Thrombotic thrombocytopenic purpura: advances in pathophysiology, diagnosis, and treatment–introduction. Semin Hematol. 2004;41:1-3.
5. Levy GG, Nichols WC, Lian EC, et al. Mutations in a member of the ADAMTS gene family cause thrombotic thrombocytopenic purpura. Nature. 2001;413:488-494.
6. Tsai HM. Deficiency of ADAMTS13 and thrombotic thrombocytopenic purpura. Blood. 2002; 100:3839-3840; author reply 3840-3842.
7. Chauhan AK, Motto DG, Lamb CB, et al. Systemic antithrombotic effects of ADAMTS13. J Exp Med. 2006;203:767-776.
8. Banno F, Kokame K, Okuda T, et al. Complete deficiency in ADAMTS13 is prothrombotic, but it alone is not sufficient to cause thrombotic thrombocytopenic purpura. Blood. 2006;107:3161-3166.
9. Dong JF, Moake JL, Bernardo A, et al. ADAMTS-13 metalloprotease interacts with the endothelial cell-derived ultra-large von Willebrand factor. J Biol Chem. 2003;278:29633-29639.
10. Dong JF. Cleavage of ultra-large von Willebrand factor by ADAMTS-13 under flow conditions. J Thromb Haemost. 2005;3:1710-1716.
11. Donadelli R, Orje JN, Capoferri C, Remuzzi G, Ruggeri ZM. Size regulation of von Willebrand factor-mediated platelet thrombi by ADAMTS13 in flowing blood. Blood. 2006;107:1943-1950.
12. Uemura M, Tatsumi K, Matsumoto M, et al. Localization of ADAMTS13 to the stellate cells of human liver. Blood. 2005;106:922-924.
13. Kato S, Matsumoto M, Matsuyama T, Isonishi A, Hiura H, Fujimura Y. Novel monoclonal antibody-based enzyme immunoassay for determining plasma levels of ADAMTS13 activity. Transfusion. 2006;46:1444-1452.
14. Tsuji S, Sugimoto M, Miyata S, Kuwahara M, Kinoshita S, Yoshioka A. Real-time analysis of mural thrombus formation in various platelet aggregation disorders: distinct shear-dependent roles of platelet receptors and adhesive proteins under flow. Blood. 1999;94:968-975.
15. Matsui H, Sugimoto M, Mizuno T, et al. Distinct and concerted functions of von Willebrand factor and fibrinogen in mural thrombus growth under high shear flow. Blood. 2002;100:3604-3610.
16. Sugimoto M, Matsui H, Mizuno T, et al. Mural thrombus generation in type 2A and 2B von Willebrand disease under flow conditions. Blood. 2003;101:915-920.
17. Mizuno T, Sugimoto M, Matsui H, Hamada M, Shida Y, Yoshioka A. Visual evaluation of blood coagulation during mural thrombogenesis under high shear flow. Thromb Res. 2007; Sep 25 [Epub ahead of print].
18. Siedlecki CA, Lestini BJ, Kottke-Marchant KK, Eppell SJ, Wilson DL, Marchant RE. Shear-dependent changes in the three-dimensional structure of human von Willebrand factor. Blood. 1996;88:2939-2950.
19. Nishio K, Anderson PJ, Zheng XL, Sadler JE. Binding of platelet glycoprotein Ibalpha to von Willebrand factor domain A1 stimulates the cleavage of the adjacent domain A2 by ADAMTS13. Proc Natl Acad Sci U S A. 2004;101:10578-10583.
20. Gao W, Anderson PJ, Majerus EM, Tuley EA, Sadler JE. Exosite interactions contribute to tension-induced cleavage of von Willebrand factor by the antithrombotic ADAMTS13 metalloprotease. Proc Natl Acad Sci U S A. 2006;103:19099-19104.

ELSEVIER

EXPERIMENTAL HEMATOLOGY

Experimental Hematology 35 (2007) 947–956

# Adiponectin binds to chemokines via the globular head and modulates interactions between chemokines and heparan sulfates

Hiroaki Masaie[a], Kenji Oritani[a], Takafumi Yokota[a], Isao Takahashi[a], Takahiro Shirogane[a], Hidetoshi Ujiie[a], Michiko Ichii[a], Norimitsu Saitoh[a], Tetsuo Maeda[a], Rie Tanigawa[a], Kazumasa Oka[b], Yoshihiko Hoshida[b], Yoshiaki Tomiyama[a], and Yuzuru Kanakura[a]

[a]*Department of Hematology and Oncology, Osaka University Graduate School of Medicine, Osaka, Japan;* [b]*Department of Pathology, Osaka University Graduate School of Medicine, Osaka, Japan*

(Received 12 April 2006; revised 15 March 2007; accepted 15 March 2007)

***Objective.*** **Adiponectin, a fat cell–derived protein, has been attracting considerable attention because of its antidiabetic and antiatherogenic activities. The aim of the present study is to identify molecules physiologically associating with adiponectin and to understand how the protein displays diverse biological activities.**

***Materials and Methods.*** **We used an expression cloning method combined with enzyme-linked immunosorbent assay to clone adiponectin-binding proteins from the MS-5 complementary DNA library.**

***Results.*** **We successfully isolated two chemokines, stromal cell–derived factor-1 (SDF-1) and CCF18, and verified that adiponectin bound to them via its globular head. Adiponectin bound with various chemokines in vitro, such as macrophage-inflammatory protein-1α (MIP-1α), RANTES, and monocyte chemoattractant protein-1 (MCP-1), suggesting that the protein had a feature commonly to bind to the chemokine family. The middle part of chemokines, dispensable for interacting with their receptors, was found to be important for the adiponectin binding. Although the interaction of adiponectin to SDF-1 affected neither the SDF-1–CXCR4 binding nor the SDF-1 signaling in Jurkat cells, adiponectin and heparin mutually interfered in their association to SDF-1 and MCP-1 in vitro, implying that their association might influence the distribution of adiponectin and SDF-1 in inflammatory sites. Indeed, both adiponectin and SDF-1 was positively immunostained in vascular walls in guts from acute graft-vs-host disease patients. In addition, peripheral blood of adiponectin-deficient mice contained more hematopoietic progenitors than that of wild-type mice.**

***Conclusion.*** **Adiponectin may be involved in regulation of inflammation via binding to specific chemokines. Additionally, the interaction possibly enables adiponectin to gather and play its role in inflammatory sites.** © **2007 International Society for Experimental Hematology. Published by Elsevier Inc.**

Adiponectin is exclusively synthesized by adipocytes and abundantly present in human plasma, with concentrations ranging from 3 to 30 μg/mL [1]. Structurally, adiponectin consists of a nonhelical variable region, a collagen-like domain, and a C-terminal globular domain. On the basis of primary amino acid sequence and domain structure, adiponectin is similar to complement C1q, a member of the soluble defense collagen family [2]. Its globular domain also has a striking structural homology to tumor necrosis factor-α (TNF-α) members when analyzed with x-ray crystallography [3]. These facts have suggested an evolutionary link of adiponectin with the two families.

With regard to physiological roles of adiponectin, experimental data have proposed that adiponectin participates in development of insulin resistance and atherosclerosis. Adiponectin is reduced in the serum of patients with obesity [1], diabetes [4], and coronary artery diseases [5]. In animal models, adiponectin-deficient mice exhibit increased insulin resistance in high-fat diet conditions [6]. Severe neointimal thickening and increased proliferation of vascular smooth muscle cells have been demonstrated

Offprint requests to: Kenji Oritani, M.D., Department of Hematology and Oncology, Graduate School of Medicine, Osaka University, 2-2 Yamadaoka, Suita City, Osaka 565-0871 Japan; E-mail: oritani@bldon.med.osaka-u.ac.jp

0301-472X/07 $–see front matter. 
doi: 10.1016/j.exphem.2007.03.010

in mechanically injured arteries of adiponectin-deficient mice [7]. Atherosclerosis of apo-E–deficient mice is improved by overexpression of adiponectin [8]. Although the mechanisms through which adiponectin exerts its actions are largely unknown and controversial, adiponectin has been shown to inhibit the production and action of TNF-α [9]. In addition, a series of our studies have demonstrated that adiponectin has anti-inflammatory effects, such as inhibition of lymphocyte production and reduction of phagocytic activity [10].

Adiponectin can bind to several secreted or cell surface proteins. Two adiponectin receptors, AdipoR1 and AdipoR2, recognize the globular head and thereby transduce signals, which increase insulin sensitivity [11]. Adiponectin acts as a platelet-derived growth factor–BB-binding protein and regulates growth factor–induced postreceptor signals in vascular smooth muscle cells [12]. T-cadherin, a glycosylphosphatidylinositol-anchored extracellular protein, as well as some types of collagens, can also recognize adiponectin [13]. Information regarding adiponectin-binding proteins has been growing and has been gradually enabling us to discuss how biological activities of adiponectin are transmitted. To identify adiponectin-binding proteins exhaustively, we established a modified two-step expression cloning to identify secreted proteins capable of binding to adiponectin [14]. We now report that adiponectin binds to chemokines, including stromal cell-derived factor-1 (SDF-1) and CCF18, via its globular head. Adiponectin interferes with heparan-sulfate on binding to chemokines, and vice versa in vitro. We also discuss physiological roles of adiponectin-chemokine interactions from the view of protein localization.

## Materials and methods

*Cells and reagents*

A human embryonic kidney cell line (293T), a mouse fibroblast cell line (COS), a mouse stromal cell clone (MS-5), and a cervix adenocarcinoma (HeLa) were maintained in Dulbecco's modified Eagle's medium (Nakarai Tesque, Kyoto, Japan) supplemented with 10% fetal calf serum (FCS; GIBCO, Grand Island, NY, USA). A human T-lymphoma cell line (Jurkat) and a human promonocytic cell line (THP-1) were maintained in RPMI-1640 (Nakarai Tesque) supplemented with 10% FCS.

Recombinant full-length human adiponectin, recombinant fusion protein composed of globular domain of murine adiponectin and glutathione-S-transferase (GST) (gAdiponectin-GST) were produced in bacteria and purified as described previously [1,6]. Recombinant proteins of human SDF-1, human macrophage-inflammatory protein-1α (MIP-1α), human monocyte chemoattractant protein-1 (MCP-1), human regulated upon activation, normal T cell expressed and secreted (RANTES), and murine CCF18 were purchased from PeproTech (Rocky Hill, NJ, USA). Goat polyclonal antibodies against SDF-1, MIP-1α, MCP-1, RANTES, or CCF18 were purchased from Santa Cruz Biotechnology (Santa Cruz, CA, USA). A monoclonal antibody against human CXCR4 was purchased from R & D Systems (Minneapolis, MN, USA). A mouse monoclonal antibody (clone HPC4) to protein C was purchased from Roche (Indianapolis, IN, USA). Biotinylated goat anti-human immunoglobulin (Ig) and biotinylated goat anti-mouse IgG were purchased from Vector Laboratories, Inc (Burlingame, CA, USA). Fluorescein isothiocyanate (FITC)–labeled goat F(ab')2 anti-human immunoglobulin (Ig) was purchased from Southern Biotechnology Associates, Inc (Birmingham, AL, USA). FITC-labeled goat anti-mouse (Ig) was purchased from BD Pharmingen (San Diego, CA, USA).

*Plasmid constructs*

Plasmids containing SDF-1 and CCF18 cDNAs were kindly provided by Dr. Nagasawa (Kyoto University, Kyoto, Japan) and Dr. Miyajima (Tokyo University, Tokyo, Japan), respectively [15,16]. Deletion mutants of SDF-1 and CCF18 were generated by polymerase chain reaction (PCR) methods and sequenced (primer sequences are available upon request).

*Plate binding assay (enzyme-linked immunosorbent assay)*

Recombinant adiponectin or gAdiponectin-GST (10 μg/mL) was fixed on a microtiter tray at 4°C overnight. After washing with 50 mM Tris-buffered saline containing 0.1% bovine serum albumin (BSA) and 0.05% Tween 20, nonspecific binding was blocked by 5% BSA at room temperature for 2 hours. After washing, appropriate concentrations of the indicated Ig-fusion proteins were incubated at room temperature for 2 hours. After washing, the bound Ig-fusion proteins were detected with enzyme-linked immunosorbent assay (ELISA) using biotinylated anti-human Ig and avidin-biotin-alkaline phosphatase complex (ABC; Vector, Burlingame, CA, USA). Enzyme-substrate reaction was performed with ELISA amplification system (Life Technologies, Gaithersburg, MD, USA) according to manufacturer's instructions. In other experiments, recombinant SDF-1, MIP-1α, MCP-1, RANTES, or CCF18 (1 μg/mL) was coated on a microtiter tray. After 100 μL recombinant adiponectin (0.5 μg/mL) was incubated, the bound adiponectin was detected by mouse anti-human adiponectin antibody (ANOC 9104), followed by biotinylated anti-mouse Ig and ABC. In addition, serum concentration of SDF-1 was quantified using Cytoscreen ELISA kit (Biosource, Kamerilo, CA, USA) according to manufacturer's instructions.

*Precipitation and Western blot*

Recombinant gAdiponectin-GST or GST was incubated with Glutathione-Sepharose 4B (Amersham Pharmacia Biotech, Uppsala, Sweden) for 2 hours at 4°C. The gAdiponectin-GST– or GST-bound Sepharoses were treated with 5% BSA to block nonspecific binding, then rotated with the indicated chemokines for 2 hours at 4°C. In some experiments, recombinant SDF-1 or MCP-1 was incubated with heparin-immobilized Sephadex (Pierce, Rockford, IL, USA) for 2 hours at 4°C. After washing, the absorbed proteins were released by boiling in sample buffer containing 2-mercaptoethanol. The precipitates were subjected to sodium dodecyl sulphate-polyacrylamide gel electrophoresis. Proteins were electrophoretically transferred onto a polyvinylidene difluoride membrane (Immobilon, Millipore Corp., Bedford, MA, USA). After blocking immunoblotting was performed with an appropriate antibody. Immunoreactive proteins were then visualized with the enhanced chemiluminescence detection system (DuPont NEN, Boston, MA, USA).

*Chemotaxic assay*

Migration of Jurkat cells was assessed in Transwell trays with 6-mm–diameter chambers and membrane pore size of 5 μm (Kurabo, Osaka, Japan). To lower wells, 300 μL RPMI-1640 medium containing SDF-1 (or plus adiponectin) was added. To upper wells, 100 μL suspension of Jurkat cells at $1 \times 10^7$ cells/mL was added. After 3 hours of incubation at 37°C, cells that migrated to the lower wells were counted.

*Intracellular calcium measurement*

Jurkat cells were suspended in RPMI-1640 and loaded with Fluo-3-AM (Molecular Probes, Eugene, OR, USA) at 2 μM for 20 minutes at room temperature. After stimulation with SDF-1, the intercellular Fluo-3-AM fluorescence signals were analyzed by F-3000 fluorescence spectrophotometer (Hitachi, Ltd., Tokyo, Japan) with an excitation light of 485 nm and an emission light of 530 nm.

*Flow cytometry*

The binding capacity of SDF-1 to CXCR4 and the surface expression of CXCR4 were analyzed with flow cytometry analysis as described previously [17]. The stained cells were analyzed with FACSort (Becton Dickinson, Mountain View, CA, USA).

*Detection of metalloproteinase-9 mRNA*

Metalloproteinase-9 (MMP-9) and β-actin mRNAs were quantified by reverse transcription PCR as described previously [18]. PCR reaction was performed with primers as listed below; 5′-AAGATGCTGCTGTTCAGCGGG-3′ and 5′-GTCCTCAGGGCACTGCAGGAT-3′ for MMP-9; 5′-CCATCCTCCGTCTGGACCTG-3′ and 5′-GTAACAGTCCGCCTAGAAGC-3′ for β-actin.

*Assays of colony formation*

To assess the colony formation of hematopoietic progenitor cells, methylcellulose progenitor assays were performed using a modification of the technique described previously [9]. Briefly, mononuclear cells were isolated from peripheral blood with Ficoll-Hypaque (Seromed, Hamburg, Germany) density gradient centrifugation and plated in methylcellulose medium (MethoCult M3434; StemCell Technologies, Vancouver, Canada) with 3 U/mL erythropoietin, 50 ng/mL stem cell factor, 10 ng/mL interleukin-3, and 10 ng/mL interleukin-6. Cultures were set up in triplicate and incubated in a humidified atmosphere at 37°C and 5% $CO_2$ for 7 days.

*Immunohistochemical staining for adiponectin*

Colon biopsies were carried out from patients who had severe diarrhea after bone marrow transplantation. The biopsy samples were embedded in paraffin. Adiponectin immunohistochemical staining was performed using antibodies against human adiponectin or SDF-1, as described previously [19]. Normal mouse serum was used for a negative control staining. For detection of endothelial cells, anti-CD34 antibody was used.

## Results

*Cloning of adiponectin-binding molecules*

To identify adiponectin-interacting molecules, we conducted a two-step expression cloning strategy as illustrated in Figure 1A. MS-5 stromal cells were characterized as an

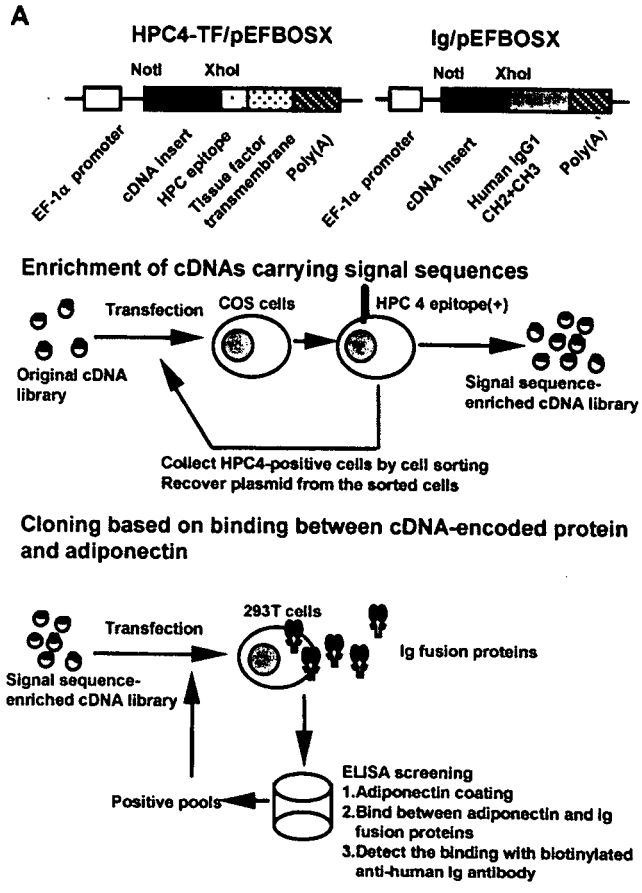


B

| Screened library | Cloned molecule | Number of clones |
|---|---|---|
| MS-5 | SDF-1 | 6 |
| | CCF18 | 1 |

**Figure 1.** Isolation of clones whose cDNAs encoded secreted proteins capable of binding to adiponectin. (A) Two-step cloning strategy. cDNAs from MS-5 library with signal sequence were first enriched with the signal sequence trap method, and then the signal sequence-enriched cDNA library was screened based on the ability to recognize adiponectin with enzyme-linked immunosorbent assay (ELISA) technique. (B) Cloned molecules. Seven individual clones were isolated with this cloning strategy. Six clones carried 5′-portion cDNA of stromal-derived factor–1 (SDF-1) and 1 clone carried CCF18 cDNA.

adiponectin-responsive preadipocyte cell line, and were assumed to secrete adiponectin-related molecules [20]. Their 5′-portion cDNAs were cloned into at NotI and XhoI sites of the HPC4-TF/pEFBOSX vector. We transfected the library into COS cells and recovered plasmids from HPC4-positive cells, which had been collected by cell sorting. Much higher percentage of transfectants with plasmids prepared from the three-times sorted cells showed positive staining for the HPC4 epitope tag than those with original cDNA library (data not shown), indicating that cDNAs carrying signal sequences could be enriched successfully. We then transferred the cDNA inserts of the signal

sequence-enriched library into the Ig/pEFBOSX vector. We picked up 2000 individual *Escherichia coli* colonies from the signal-sequence–enriched library in the Ig/pEFBOSX vector. Each plasmid pool was transfected into 293T cells, and their supernatants were harvested 3 days after the transfection. The ELISA technique where adiponectin was coated on the tray was used to identify pools, which contained plasmids capable of producing adiponectin-binding Ig fusion proteins. As summarized in Figure 1B, seven individual clones whose Ig fusion proteins had this property were isolated. Six clones carried 5′-portion cDNA of SDF-1 and one clone carried CCF18 cDNA [15,16]. SDF-1 is a CXC-type chemokine, and CCF18 is a CC-type chemokine. Both are known to have signal sequences and to be secreted. Therefore, we identified two chemokines as potential interaction molecules with adiponectin using our established expression cloning.

*Binding of SDF-1 and CCF18 to adiponectin*

Ig fusion proteins of entire cording region of SDF-1 (SDF-1–Ig) and CCF18 (CCF18-Ig) were used to show their direct binding to adiponectin. An ELISA assay system detecting the bound Ig fusion proteins revealed that both SDF-1–Ig and CCF18-Ig could bind to plate-coated recombinant human adiponectin (Fig. 2). Similar binding of SDF-1–Ig and CCF18-Ig was observed when recombinant globular domain of murine adiponectin was fixed on the tray. However, CD44-Ig could recognize neither full-length nor globular domain of adiponectin. The binding to plate-coated BSA was low, and there was no difference among SDF-1–Ig, CCF18-Ig, and CD44-Ig. Therefore, SDF-1–Ig and CCF18-Ig specifically bind to both human and murine adiponectin, and globular domain of adiponectin is enough for their recognition.

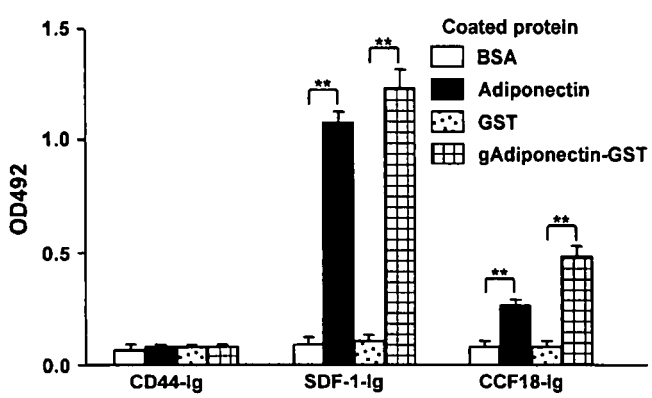


**Figure 2.** Adiponectin binds to stromal-derived factor–1 (SDF-1) and CCF18 via its globular head. Bovine serum albumin (BSA; open columns), recombinant adiponectin (closed columns), glutathione-S-transferase (GST; dotted columns) or gAdiponectin-GST (cross stripes columns) protein (10 μg/mL) was fixed on a microtiter tray at 4°C overnight. After blocking, SDF-1–immunoglobulin (Ig) or CCF18-Ig (1 μg/mL) was incubated at room temperature for 2 hours. The bound Ig-fusion proteins were detected with enzyme-linked immunosorbent assay (ELISA) using biotinylated anti-human Ig and avidin-biotin-alkaline phosophatase complex. Data are shown as mean ± SD of $OD_{492}$ in tripricated samples. Statistically differences from control values are shown with two asterisks ($p < 0.01$). Similar results were obtained in three independent experiments.

To determine which parts of SDF-1 and CCF18 are involved in the binding, we made several deletion mutants of SDF-1 and CCF18 where both chemokines were divided into three parts: the amino-terminal part (N), the middle part (M), and the carboxyl-terminal part (C) (Fig. 3A). Similar to SDF-1–Ig, SDF(N + M) –Ig and SDF(M + C) –Ig, which contained middle part of SDF-1, could bind to adiponectin (Fig. 3B). However, SDF(N)-Ig, which contains only N-terminal portion of SDF-1, and SDF(C)-Ig, which contains only C-terminal portion of SDF-1 failed to bind to adiponectin. In parallel experiments, CCF18-Ig, CCF18(N + M)-Ig and CCF18(M + C)-Ig, but not CCF18(N)-Ig or CCF18(C)-Ig, could bind to adiponectin. Therefore, the middle portion of SDF-1 (AA 19–53) and CCF18 (AA 36–78) are important for the binding to adiponectin.

*Adiponectin binds to diverse chemokines in vitro*

Adiponectin binds to SDF-1, a CXC-type chemokine, and CCF18, a CC-type chemokine [15,16]. These facts indicated that adiponectin might recognize a broad range of chemokines. We evaluated the binding of recombinant adiponectin to the plate-coated chemokines with ELISA as shown in Figure 4A. Adiponectin significantly recognized RANTES and MCP-1 as well as SDF-1 and CCF18. Although the binding between adiponectin and MIP-1α was not very impressive, the ELISA data indicated a statistically significant difference ($p < 0.05$). After gAdiponectin-GST fusion protein was immobilized on glutathione Sephadex, the binding of chemokines to adiponectin was evaluated with Western blot. SDF-1 in the precipitate was detected faintly when 100 ng SDF-1 was treated with gAdiponectin-GST–fixed glutathione Sephadex (Fig. 4B). Stronger band was observed when 500 ng SDF-1 was applied. In contrast, no binding of SDF-1 was detected in the precipitates of GST-fixed glutathione Sephadex. RANTES and MCP-1 were detected in the precipitates of gAdiponectin-GST–fixed glutathione Sephadex when they were applied at 500 ng. However, binding of MIP-1α to gAdiponectin-GST–fixed glutathione Sephadex was under detectable level. The intensity of each band was consistent to the results obtained by ELISA assay. Therefore, adiponectin has a general feature to bind to the chemokine family, although the affinity is different.

*Adiponectin does not affect chemokine-receptor interactions*

We intended to investigate the influence of adiponectin on chemokine functions. We used Jurkat cells, which express CXCR4, a SDF-1 receptor, abundantly. Flow cytometry analysis clearly depicted the binding of SDF-1–Ig to Jurkat cells (Fig. 5A). Premixture of adiponectin with SDF-1–Ig did not reduce binding, while a monoclonal antibody

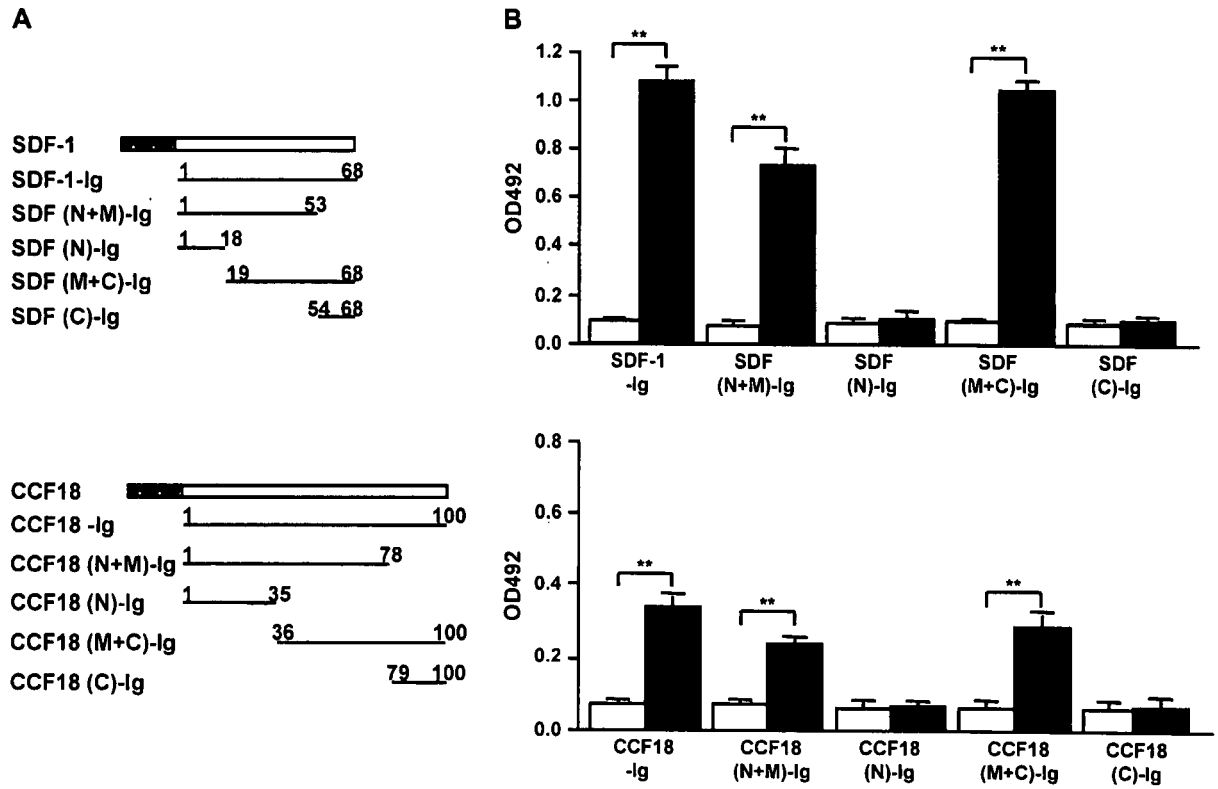


**Figure 3.** Determination of adiponectin-binding sites on chemokines. (**A**) Scheme of deleted stromal-derived factor–1 (SDF-1)– or CCF18-immunoglobulin (Ig) fusion proteins. The cDNA fragments of SDF-1 and CCF18 were amplified by polymerase chain reaction with primers as described in Materials and Methods, and cloned into the Ig/pEFBOSX vector. Amino acid numbers of mature proteins are shown. (**B**) Plasmids for producing the indicated Ig fusion proteins were transfected to 293T cells with calcium phosphate precipitation methods. After 3 days of cultures, each supernatant was collected and subjected to Western blots probed with anti-human Ig antibody. Ten micrograms per milliliter of BSA (open columns) or adiponectin (closed columns) was fixed on a microtiter tray at 4°C overnight. After blocking, supernatants containing each deleted SDF-1-Ig or CCF18-Ig were incubated at room temperature for 2 hours. The bound Ig-fusion proteins were detected with enzyme-linked immunosorbent assay using biotinylated anti-human Ig and avidin-biotin-alkaline phosophatase complex. Data are shown as mean ± SD of $OD_{492}$ in tripricated samples. Statistically differences from control values are shown with two asterisks ($p < 0.01$). Similar results were obtained in three independent experiments.

recognizing CXCR4 inhibited the binding significantly. We next examined the chemotaxis of Jurkat cells by recombinant SDF-1. SDF-1 induced the migration activity and >40% of the cells moved to lower chambers within 30 minutes (Fig. 5B). While the migration was strongly abrogated by an anti-CXCR4 antibody, 10 to 20 μg/mL adiponectin showed little or no inhibitory or enhancing effects. Moreover, the Ca influx induced by recombinant SDF-1 was not affected by the addition of adiponectin (Fig. 5C). In the case of MCP-1, adiponectin failed to affect MCP-1–induced migration activity in THP-1 cells (data not shown). Therefore, adiponectin dose not influence chemokine–receptor interactions.

*Adiponectin and heparan-sulfate proteoglycans influence each other on the binding to chemokines*

Chemokines have positively charged domains, which are important to bind with heparan-sulfate proteoglycans (HSPG). The heparin-binding capacity involves in their localization and is required for their full-function in vivo [21]. We tested whether adiponectin influences the heparin-binding capacity of SDF-1 and MCP-1. Heparin Sephadex could precipitate recombinant SDF-1 and MCP-1, which were detectable with Western blot, and the binding was completely blocked by the addition of heparin (Fig. 6). When gAdiponectin was added to the mixture, SDF-1 and MCP-1 in the precipitates were decreased in a gAdiponectin dose-dependent manner (Fig. 6). Therefore, adiponectin reduces the binding capacity of chemokines to heparin.

The influence of heparin on the interaction between adiponectin and SDF-1 was evaluated using two experimental models, ELISA, and immunoprecipitation assays. When the binding of SDF-1–Ig and CCF18-Ig to adiponectin in the presence of heparin was evaluated with ELISA, their binding was completely inhibited by heparin (Fig. 7A). However, another adiponectin-binding protein, cystatin-C, recognized adiponectin even in the presence of heparin. Glutathione Sephadex was treated with gAdiponectin-GST fusion protein, and then the binding capacity of adiponectin-bearing Sephadex to recombinant SDF-1 in the presence of heparin was examined. The precipitate without heparin clearly contained SDF-1, but SDF-1 was

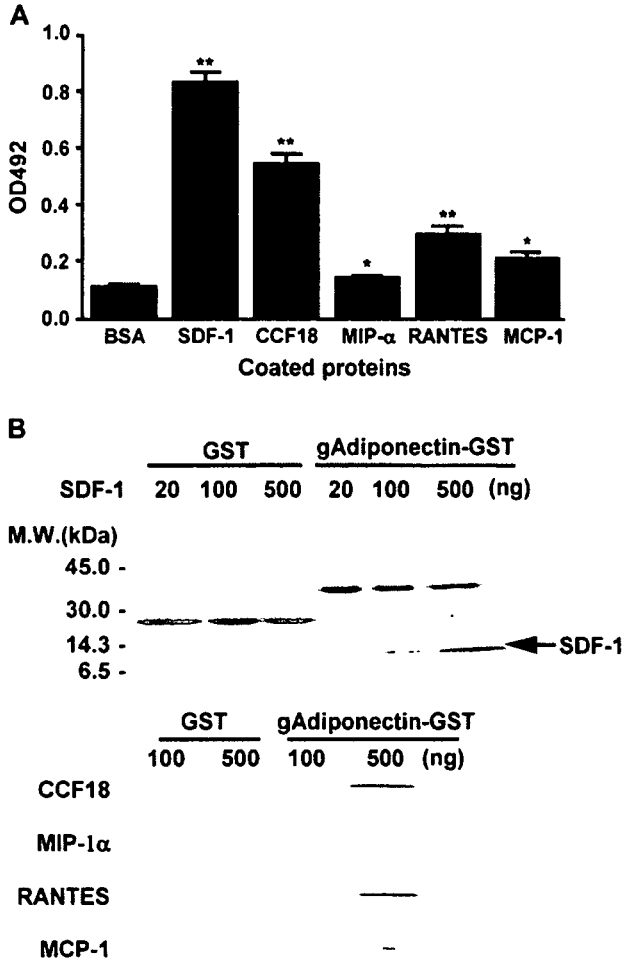


**Figure 4.** Adiponectin binds to various chemokines. (A) The indicated recombinant chemokine, stromal-derived factor–1 (SDF-1), CCF18, macrophage-inflammatory protein-1α (MIP-1α) , RANTES, or monocyte chemoattractant protein-1 (MCP-1; 1 μg/mL), was fixed on a microtiter tray at 4°C overnight. After blocking, recombinant adiponectin (0.5 μg/mL) was incubated at room temperature for 2 hours. The bound adiponectin was detected by mouse anti-human adiponectin antibody (ANOC9104), followed by enzyme-linked immunosorbent assay using biotinylated anti-mouse immunoglobulin (Ig) and avidin-biotin-alkaline phosphatase complex. Data are shown as means ± SD of $OD_{492}$ in tripricated samples. Statistically differences from control values (bovine serum albumin–coated) are shown with one ($p < 0.05$) or two ($p < 0.01$) asterisks. Similar results were obtained in three independent experiments. (B) Recombinant gAdiponectin-glutathione-S-transferase (GST) or GST was incubated with Glutathione-Sepharose 4B for 2 hours at 4°C. The gAdiponectin-GST– or GST-bound Sepharoses was mixed with the indicated chemokine, SDF-1, CCF-18, MIP-1α, RANTES, or MCP-1 for 2 hours at 4°C, and then precipitated. The precipitates were subjected to Western blots probed with appropriate antichemokine antibody.

not detected in the precipitate with heparin (Fig. 7B). Therefore, the binding between SDF-1 and adiponectin was blocked by heparin.

These results indicate that adiponectin and heparin negatively influence each other on the binding to chemokines. This implies that the HSPG–chemokine and adiponectin–chemokine interactions may implicate each other in vivo, changing the balance in accordance with physiological condition.

*Physiological roles of adiponectin in SDF-1–mediated actions*

Brule et al. [18] reported that induction of MMP-9 gene expression by SDF-1 in HeLa cells depended on cell-surface HSPG, but not on CXCR4. We then analyzed effects of adiponectin on MMP-9 gene expression induced by SDF-1 (Fig. 8). Treatment of HeLa cells with SDF-1 induced MMP-9 gene expression, and this was completely inhibited by the addition of heparin. Addition of adiponectin also inhibited SDF-1–induced MMP-9 gene expression in a dose-dependent manner. Therefore, adiponectin actually modulates functional SDF-1 activity, which depends on HSPG.

SDF-1 is also critical for the homing of hematopoietic stem cells to bone marrow [22]. In bone marrow, adipocytes, but not hematopoietic cells, produce adiponectin [20]. As shown in Figure 9, serum concentration of SDF-1 is higher in adiponectin-deficient mice than controls. In addition, peripheral blood in adiponectin-deficient mice carries more hematopoietic progenitors than that in wild-type mice. Therefore, adiponectin actually influences the localization of SDF-1 in vivo.

*Colocalization of adiponectin with SDF-1 at vascular walls in acute graft-vs-host disease gut*

Among patients who had received bone marrow transplantation, seven patients experienced severe diarrhea. These patients were diagnosed as acute intestinal graft-vs-host disease (GVHD) from their colon biopsies. We examined the localization of adiponectin and SDF-1 in inflammatory sites. Similar staining results were obtained in all patients, and we showed representative staining data (Fig. 10). Both adiponectin and SDF-1 proteins were clearly detected at vascular walls in the gut, which were positively stained with anti-CD34 antibody. In contrast, no positive cells were observed when the sections were stained with control mouse serum. Therefore, adiponectin colocalized with SDF-1 at vascular walls in the gut of patients with acute intestinal GVHD.

## Discussion

With our established two-step expression cloning strategy [14], we successfully identified SDF-1 and CCF18 as new adiponectin-binding proteins. In addition, other CC chemokines, MIP-1α, RANTES, and MCP-1 were found to associate with adiponectin while the affinity was different. Thus, adiponectin is likely to interact with various chemokines. Adiponectin could not influence the binding of SDF-1 to Jurkat cells, SDF-1–induced intracellular calcium flux, or chemotaxis, indicating that adiponectin has no effects on the interaction between SDF-1 and CXCR4 in vitro. Crump et al. [23] reported that the N-terminal eight residues of

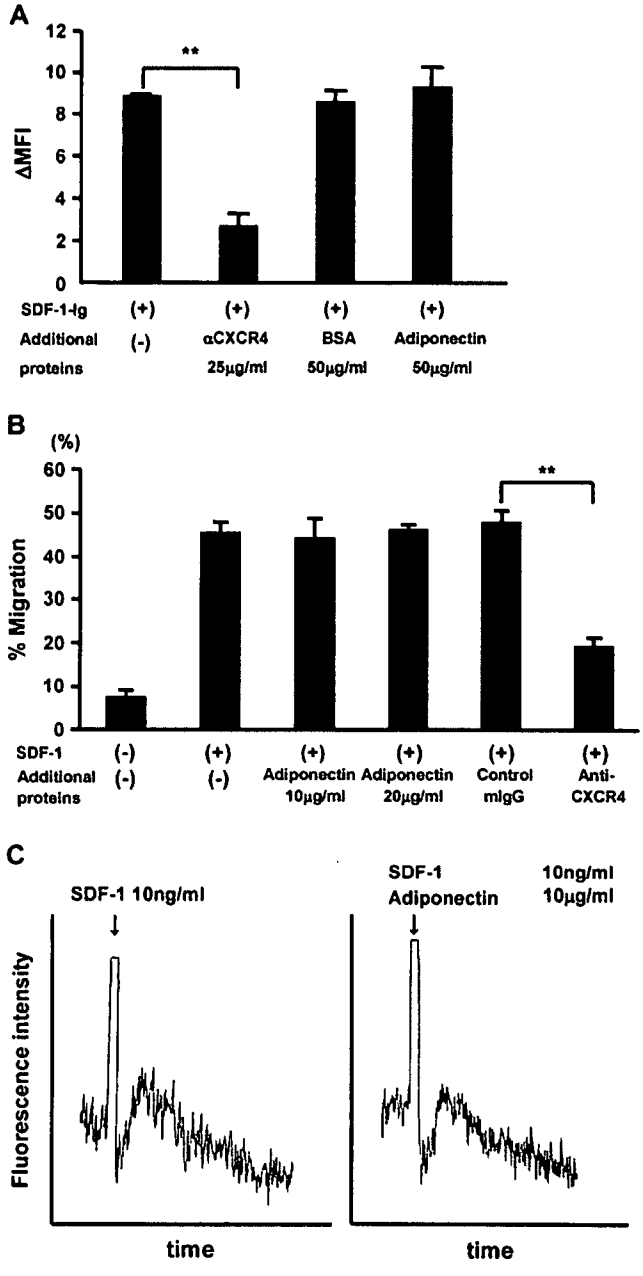


**Figure 5.** Adiponectin displays no influence on the stromal-derived factor–1 (SDF-1) signaling via its receptor CXCR4. (**A**) Binding of SDF-1–Ig to Jurkat cells. SDF-1-immunoglobulin (Ig) (1 μg/mL) with or without bovine serum albumin (BSA; 50 μg/mL) or adiponectin (50 μg/mL) was added to Jurkat cells ($1 \times 10^5$ cells) for 20 minutes at 4°C. Jurkat cells pretreated with CXCR4 antibody (25 μg/mL) were also stained with SDF-1–Ig. After washing, the bound Ig fusion proteins were detected by fluorescein isothiocyanate–labeled anti-human Ig. Δ Mean fluorescence intensity (ΔMFI) was calculated as [MFI (the indicated staining) – MFI (control staining with second antibody alone)]. Data are shown as mean ± SD in three independent experiments. Statistically significances are shown with two ($p < 0.01$) asterisks. Similar results were obtained in three independent experiments. (**B**) SDF-1–induced chemotaxic activity. To lower wells, 300 μL RPMI-1640 medium containing SDF-1 (10 ng/mL) with or without adiponectin (10 or 20 μg/mL) was added. To upper wells, 100 μL suspension of Jurkat cells ($1 \times 10^7$ cells/ml) were added. In some wells, anti-human CXCR4 antibody (5 μg/mL) or control IgG was added to upper wells. After 3 hours of incubation at 37°C, cells that migrated to the lower wells were counted. % migration was calculated as 100 × [cell number in lower wells/applied cell number]. Data are shown as mean ± SD in tripricated samples. Statistically differences from control values are shown with two ($p < 0.01$) asterisks. Similar results were obtained in two independent experiments. (**C**) SDF-1–induced Ca-influx. Fluo-3-AM–labeled Jurkat cells ($1 \times 10^6$) were stimulated with the premixtures of SDF-1 (10 ng/mL) with (right) or without (left) adiponectin (10 μg/mL). The intercellular Fluo-3-AM fluorescence signals were analyzed by F-3000 fluorescence spectrophotometer. Similar results were obtained in two independent experiments.

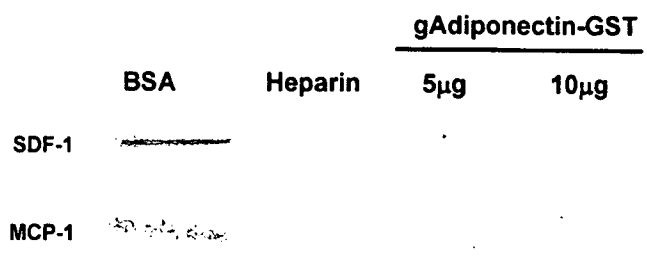


**Figure 6.** Adiponectin inhibits the binding of chemokines to heparin. The mixture samples of stromal-derived factor–1 (SDF-1) or monocyte chemoattractant protein-1 (MCP-1) (100 ng) and heparin Sephadex were precipitated in the presence of the indicated amount of gAdiponectin- glutathione-S-transferase (GST) or heparin (5 μg) for 2 hours at 4°C. After washing, the precipitates were subjected to Western blots probed with anti–SDF-1 or anti–MCP-1 antibody.

SDF-1, especially Lys-1 and Pro-2, formed an important receptor-binding site. Our ELISA using the deletion mutants of SDF-1 have revealed that N-terminal region of SDF-1 does not attribute to adiponectin-binding. Thus, the difference of the binding sites could be a reason why adiponectin fails to modify the interaction between SDF-1 and CXCR4. On the other hand, chemokines interact with HSPG and are immobilized on the surface of cells. The haptotactic gradient of the immobilized chemokines is essential for chemokine action in vivo, because chemokines carrying mutations in the HSPG-binding sites retained their activity in vitro, but not in vivo [21]. Because the binding of SDF-1 to heparin was significantly blocked by the presence of adiponectin, adiponectin may affect the localization of chemokines in vivo via the modification of their interactions with HSPG. Amara et al. [24] reported that the basic residues Lys-24, His-25, Lys-27, and Arg-41 of SDF-1, which cluster along the two first β strands, exhibit high positive potential to interact with HSPG. These regions correspond to the middle portion of SDF-1, which is important to bind to adiponectin. The residues responsible for the binding of the CC chemokines to HSPG are clusters of basic residues composed of Arg-18, Lys-19, Arg-24, Lys-49, Lys-58, and His-66 in MCP-1 [25,26] as well as Arg-18, Arg-46, and Arg-48 in MIP-1α [27]. The interesting result that the SDF-1–adiponectin binding was blocked by the addition

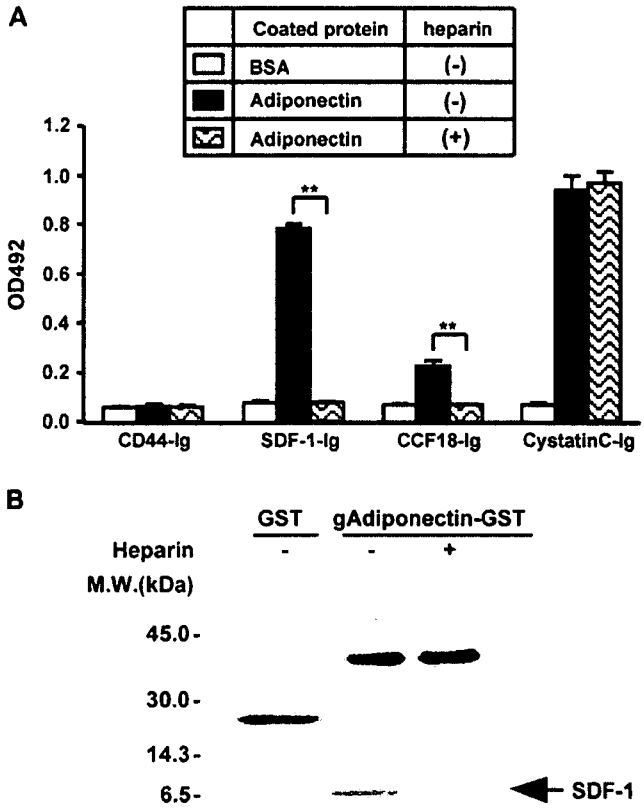


**Figure 7.** Heparin inhibits the binding of chemokines to adiponectin. (**A**) Recombinant adiponectin (10 μg/mL) was fixed on a microtiter tray at 4°C overnight. After blocking, stromal-derived factor-1 (SDF-1)–immunoglobulin (Ig), CCF18-Ig, or Cystatin-C–Ig (1 μg/mL) was incubated at room temperature for 2 hours in the presence or absence of heparin (10 μg/mL). The bound Ig-fusion proteins were detected with enzyme-linked immunosorbent assay using biotinylated anti-human Ig and avidin-biotin-alkaline phosophatase complex. Data are shown as mean (± SD of OD492 in tripricated samples. Statistically differences from control values are shown with two ($p < 0.01$) asterisks. Similar results were obtained in three independent experiments. (**B**) The mixture samples of SDF-1 and gAdponectin- glutathione-S-transferase (GST) glutathione Sephadex were precipitated in the presence or absence of heparin (10 μg/mL). The precipitates were subjected to Western blots probed with anti-SDF-1 antibody.

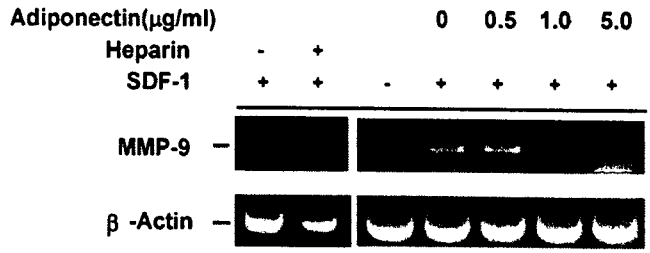


**Figure 8.** Adiponectin inhibits stromal-derived factor-1 (SDF-1)–induced metalloproteinase-9 (MMP-9) gene expression. HeLa cells in a confluent condition were stimulated with SDF-1 (10 ng/mL) in the presence or absence of heparin (1 μg/mL) or the indicated concentration of adiponectin for 8 hours. Total RNAs were prepared from the stimulated cells and subjected to reverse transcription polymerase chain reaction for MMP-9 or β-actin. Similar results were obtained in three independent experiments.

of heparin might suggest that adiponectin recognizes the cluster of basic residues on chemokines.

Our finding with respect to the mutual interference between heparin and adiponectin in the interaction with chemokines could be very important. It has been demonstrated that most chemokines bind to HSPG, which is ubiquitously expressed on the cell surface. This binding is thought to be functionally significant, and current models indicate that HSPG enhances the local concentration of chemokines in the vicinity of chemokine receptors [28]. Leukocyte migration along the endothelium surface and migration into the tissues at the site of inflammation is believed to depend on the local presentation of chemokines by HSPG. Homing of hematopoietic stem cells to bone marrow also depends on SDF-1, the localization of which is affected by HSPG. Our present observation raises the possibility that adiponectin might regulate chemokine-mediated functions in vivo by altering the distribution of chemokines.

In addition to antidiabetic and antiatherogenic properties [6,8], recent studies have provided insight into direct and/or indirect effects of adiponectin on inflammation. Adiponectin inhibits TNF-α–induced expression of vascular cell adhesion molecule -1 in endothelial cells [5]. Adiponectin also suppresses TNF-α–induced inflammatory changes via blocking nuclear factor-κB activation [29]. Additional anti-inflammatory effects of adiponectin include the suppression of leukocyte colony formation, the reduction of phagocytic activities and TNF-α secretion in lipopolysaccharide-stimulated macrophages as well as the enhancement of interleukin-10 production in cultured macrophages [9,30]. Indeed, an inverse relationship was observed between adiponectin and C-reactive protein in plasma of patients with coronary artery diseases [31]. Although anti-inflammatory effects of adiponectin are mediated in part by the counteraction against TNF-α, it is not clear how adiponectin itself inhibits systemic inflammation. In the present study, we found a new possible mechanism how adiponectin yields anti-inflammatory effects thorough interacting with several chemokines. Although adiponectin is abundant in plasma, it accumulates at the fatty streak in atherosclerotic lesion of apo-E–deficient mice as well as at the walls of the catheter-injured blood vessels [8,15]. Adiponectin is also found in interstitium of the infarcted lesions at an early stage of myocardial infarction [32]. We here described that adiponectin accumulates at vessel walls in the gut of patients with acute intestinal GVHD. The restricted localization of adiponectin under inflammatory circumstance could affect the distribution of chemokines. Conversely, chemokine–HSPG interactions could influence the adiponectin distribution. Further studies will give an answer to this possibility.

In summary, we identified chemokines as adiponectin-associated molecules. We clarified that the interaction occurs between the globular head of adiponectin and the central region of chemokines and that the interaction was blocked by heparin. In addition, we showed that adiponectin

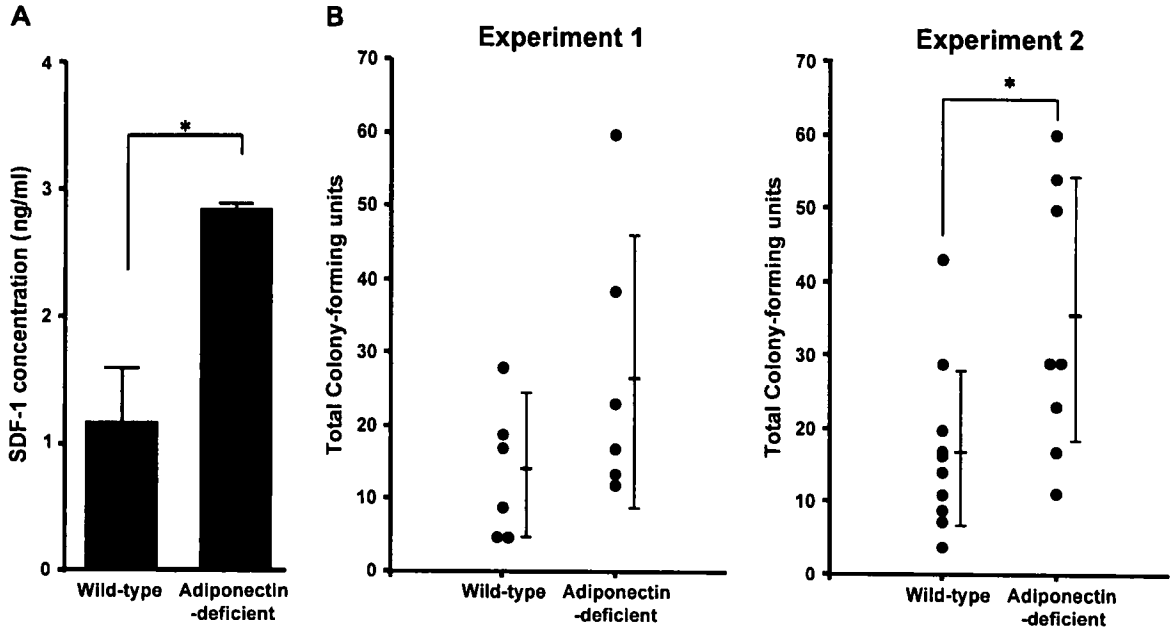


**Figure 9.** Adiponectin influences stromal-derived factor-1 (SDF-1) localization in vivo. Peripheral blood was collected from adiponectin-deficient or wild-type mice. (**A**) Serum concentration of SDF-1 was measured with Cytoscreen enzyme-linked immunosorbent assay kit. Data are shown as means (±SD in five individual mice for each group. (**B**) Mononuclear cells isolated from peripheral blood were subjected to colony assays for hematopoietic progenitors. Total colony numbers per 200 μL peripheral blood from each individual mice are shown. Statistically differences from control values are shown with one asterisk ($p < 0.05$).

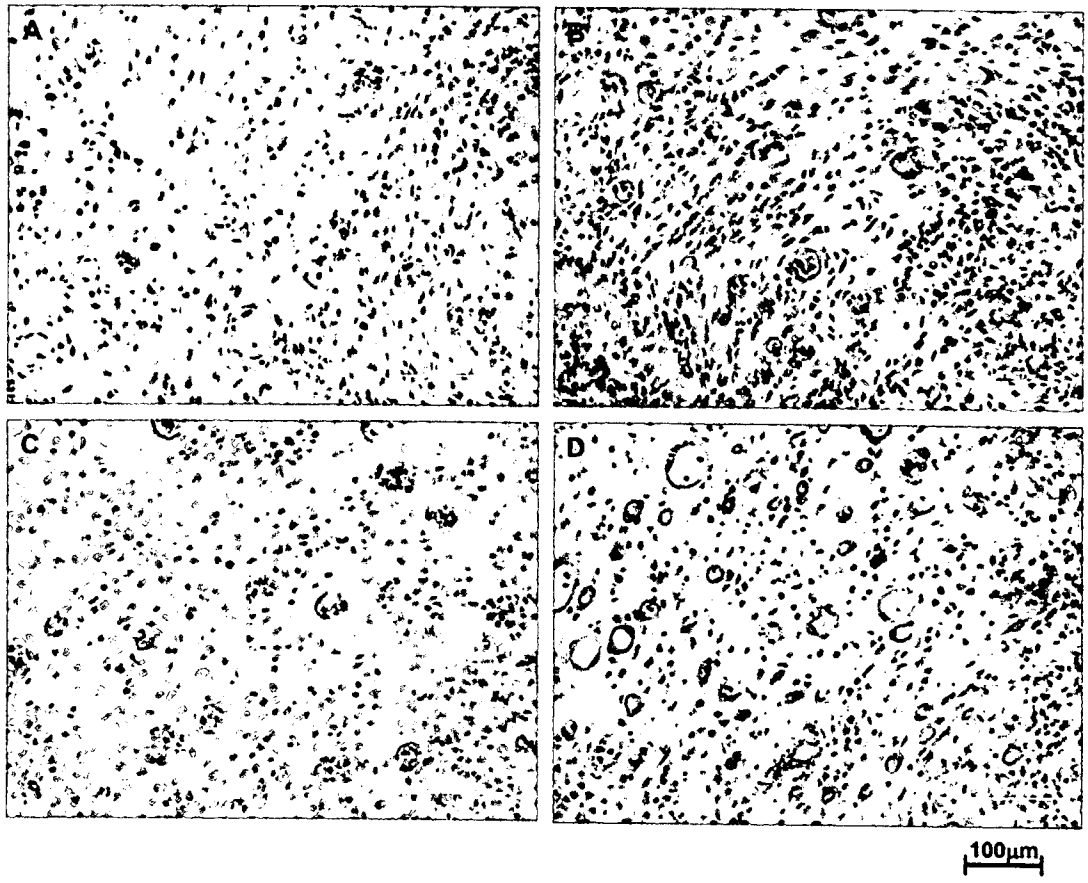


**Figure 10.** Localization of adiponectin and stromal-derived factor-1 (SDF-1) in guts of patients with acute intestinal graft-vs-host disease (GVHD). Colon sections from an acute intestinal GVHD patient who had received bone marrow transplantation were immunostained with control serum (**A**), antiadiponectin (**B**) or anti–SDF-1 antibody (**C**), or anti-CD34 antibody (**D**) (×200).

accumulates in inflammatory sites where the chemokines play a role in the recruitment of leukocytes. Although the physiological significance of adiponectin–chemokine interaction remains to be elucidated, our findings should give a new insight to understand how adiponectin implicates in diverse biological activities.

## Acknowledgments

This work was supported in part by grants from the Japan Research Foundation for Clinical Pharmacology and the Mochida Memorial Foundation for Medical and Pharmaceutical Research.

## References

1. Arita Y, Kihara S, Ouchi N, et al. Paradoxical decrease of an adipose-specific protein, adiponectin, in obesity. Biochem Biophys Res Commun. 1999;257:79–83.
2. Maeda K, Okubo K, Shimomura I, Funahashi T, Matsuzawa Y, Matsubara K. cDNA cloning and expression of a novel adipose specific collagen-like factor, apM1 (AdiPose Most abundant Gene transcript 1). Biochem Biophys Res Commun. 1996;221:286–289.
3. Shapiro L, Scherer PE. The crystal structure of a complement-1q family protein suggests an evolutionary link to tumor necrosis factor. Curr Biol. 1998;8:335–338.
4. Hotta K, Funahashi T, Arita Y, et al. Plasma concentrations of a novel, adipose-specific protein, adiponectin, in type2 diabetic patients. Arterioscler Thromb Vasc Biol. 2000;20:1595–1599.
5. Ouchi N, Kihara S, Arita Y, et al. Novel modulator for endothelial adhesion molecules. Circulation. 1999;100:2473–2476.
6. Maeda N, Shimomura I, Kishida K, et al. Diet-induced insulin resistance in mice lacking adiponectin/ACRP30. Nat Med. 2002;8:731–737.
7. Matsuda M, Shimomura I, Sata M, et al. Role of adiponectin in preventing vascular stenosis. The missing link of adipo-vascular axis. J Biol Chem. 2002;277:37487–37491.
8. Okamoto Y, Kihara S, Ouchi N, et al. Adiponectin reduces atherosclerosis in apolipoprotein E-deficient mice. Circulation. 2002;106:2767–2770.
9. Yokota T, Oritani K, Takahashi I, et al. Adiponectin, a new member of the family of soluble defense collagens, negatively regulates the growth of myelomonocytic progenitors and the functions of macrophages. Blood. 2000;96:1723–1732.
10. Yokota T, Meka CSR, Kouro T, et al. Adiponectin, a fat cell product, influences the earliest lymphocyte precursors in bone marrow cultures by activation of the cyclooxygenase-prostaglandin pathway in stromal cells. J Immunol. 2003;171:5091–5099.
11. Yamauchi T, Kamon J, Ito Y, et al. Cloning of adiponectin receptors that mediate antidiabetic metabolic effects. Nature. 2003;423:762–769.
12. Wang Y, Lam KSL, Xu JY, et al. Adiponectin inhibits cell proliferation by interacting with several growth factors in an oligomerization-dependent manner. J Biol Chem. 2005;280:18341–18347.
13. Hug C, Wang J, Ahmad NS, Bogan JS, Tsao TS, Lodish HF. T-cadherin is a receptor for hexameric and high-molecular-weight forms of Acrp30/adiponectin. Proc Natl Acad Sci. 2004;101:10308–10313.
14. Oritani K, Kincade PW. Identification of stromal cell products that interact with Pre-B cells. J Cell Biol. 1996;134:771–782.
15. Nagasawa T, Kikutani H, Kishimoto T. Molecular cloning and structure of a pre-B-cell growth-stimulating factor. Proc Natl Acad Sci USA. 1994;91:2305–2309.
16. Hara T, Bacon KB, Cho LC, et al. Molecular cloning and functional characterization of a novel member of the C-C chemokine family. J Immunol. 1995;155:5352–5358.
17. Roland J, Murphy BJ, Ahr B, et al. Role of the intracellular domains of CXCR4 in SDF-1-mediated signaling. Blood. 2003;101:399–406.
18. Brule S, Charnaux N, Sutton A, et al. The shedding of syndecan-4 and syndecan-1 from Hela cells and human primary macrophages is accelerated by SDF-1/CXCL12 and mediated by the matrix metalloproteinase-9. Glycobiology. 2006;16:488–501.
19. Okamoto Y, Arita Y, Nishida M, et al. An adipocyte-derived plasma protein, adiponectin, adheres to injured vascular walls. Horm Metab Res. 2000;32:47–50.
20. Yokota T, Meka CSR, Medina KL, et al. Paracrine regulation of fat cell formation in bone marrow cultures via adiponectin and prostaglandins. J Clin Invest. 2002;109:1303–1310.
21. Proudfoot AEI, Handel TM, Johnson Z, et al. Glycosaminoglycan binding and oligomerization are essential for the in vivo activity of certain chemokines. Proc Natl Acad Sci U S A. 2003;100:1885–1890.
22. Aiuti A, Webb IJ, Bleul C, et al. The chemokine SDF-1 is a chemoattractant for human CD34+ hematopoietic progenitor cells and provides a new mechanism to explain the mobilization of CD34+ progenitors to peripheral blood. J Exp Med. 1997;185:111–120.
23. Crump MP, Gong JH, Loetscher P, et al. Solution structure and basis for functional activity of stromal cell-derived factor-1; dissociation of CXCR4 activation from binding and inhibition of HIV-1. EMBO J. 1997;16:6996–7007.
24. Amara A, Lorthioir O, Valenzuela A, et al. Stromal cell-derived factor-1 alpha associates with heparan sulfates through the first beta-strand of the chemokine. J Biol Chem. 1999;274:23916–23925.
25. Lau EK, Paavola CD, Johnson Z, et al. Identification of the glycosaminoglycan binding site of the CC chemokine, MCP-1: implications for structure and function in vivo. J Biol Chem. 2004;279:22294–22305.
26. Chakravarty L, Rogers L, Quach T, Breckenridge S, Kolattukudy PE. Lysine 58 and histidine 66 at the C-terminal alpha-helix of monocyte chemoattractant protein-1 are essential for glycosaminoglycan binding. J Biol Chem. 1998;273:29641–29647.
27. Koopmann W, Krangel MS. Identification of a glycosaminoglycan-binding site in chemokine macrophage inflammatory protein-1 alpha. J Biol Chem. 1997;272:10103–10109.
28. Hoogewerf AJ, Kuschert GSV, Proudfoot AEI, et al. Glycosaminoglycans mediate cell surface oligomerization of chemokines. Biochemistry. 1997;36:13570–13578.
29. Ouchi N, Kihara S, Arita Y, et al. Adiponectin, an-adipocyte-derived plasma protein, inhibits endothelial NF-kB signaling through a cAMP-dependent pathway. Circulation. 2000;102:1296–1301.
30. Kumada M, Kihara S, Ouchi N, et al. Adiponectin specifically increased tissue inhibitor of matelloproteinase-1 through interleukin-10 expression in human macrophages. Circulation. 2004;109:2046–2049.
31. Ouchi N, Kihara S, Funahashi T, et al. Reciprocal association of C-reactive protein with adiponectin in blood stream and adipose tissue. Circulation. 2003;107:671–674.
32. Ishikawa Y, Akasaka Y, Ishii T, et al. Changes in the distribution pattern of gelatin-binding protein of 28 kDa (adiponectin) in myocardial remodelling after ischaemic injury. Histopathology. 2003;42:43–52.

# Inherited and *de novo* mutations of *ADAMTS13* in a patient with Upshaw-Schulman syndrome

K. KOKAME, * Y. AOYAMA, † M. MATSUMOTO, ‡ Y. FUJIMURA‡ and T. MIYATA*

**National Cardiovascular Center Research Institute, Suita, Osaka; †Department of Hematology, Seichokai Fuchu Hospital, Izumi, Osaka; and ‡Department of Blood Transfusion Medicine, Nara Medical University, Kashihara, Nara, Japan*

**To cite this article:** Kokame K, Aoyama Y, Matsumoto M, Fujimura Y, Miyata T. Inherited and *de novo* mutations of *ADAMTS13* in a patient with Upshaw-Schulman syndrome. *J Thromb Haemost* 2008; **6**: 213–5.

Upshaw-Schulman syndrome (USS) is a congenital thrombotic and hemorrhagic diathesis characterized by a deficient activity of plasma von Willebrand factor (VWF)-cleaving protease, ADAMTS13 [1–8]. Some patients with USS develop severe jaundice soon after birth as their first symptom, and some are almost asymptomatic during childhood to adolescence, unless they have precipitating factors such as infection or pregnancy. The pathological condition of USS belongs to thrombotic thrombocytopenic purpura (TTP), which is characterized by thrombocytopenia, hemolytic anemia and microvascular thrombosis. USS, therefore, is also called congenital TTP. Most cases of TTP result from acquired deficient activity of ADAMTS13 caused by the advent of autoantibodies that inhibit the ADAMTS13 activity. In contrast, patients with USS do not carry such inhibitory antibodies in their plasma, and suffer from USS because of the compound heterozygous or homozygous mutations of the *ADAMTS13* gene. More than 80 mutations of *ADAMTS13* have been identified in patients with USS. Here, we report a first case with *de novo* mutations of *ADAMTS13*.

Patient *P* (II-2 in Fig. 1A) is the second child of unrelated Japanese parents (I-1 and I-2). The first child (II-1) was spontaneously aborted from an unknown cause at 6 weeks of pregnancy, while the fourth child (II-4) was aborted by umbilical coiling at 22 weeks. The parents and the third child (II-3) are apparently healthy. The patient showed moderate hyperbilirubinemia soon after birth and received phototherapy without exchange blood transfusion. On the occasion of catching cold at 3 years of age, he developed thrombocytopenia, microangiopathic hemolytic anemia, and renal insufficiency. He was diagnosed as having TTP and treated with fresh frozen plasma (FFP) infusions. Thereafter, he repeated these episodes several times a year, and each time he soon recovered with FFP infusions. At 21 years of age, he developed a hallmark of TTP, consisting of thrombocytopenia, microangiopathic hemolytic anemia, neurological dysfunction, renal failure and fever. He started taking prophylactic infusions of FFP (4–8 ml $kg^{-1}$ body weight) every 2 weeks.

The plasma ADAMTS13 activities of the family members, measured by the method based on VWF-multimer analysis [1,9], are shown under each symbol in Fig. 1A. The ADAMTS13 activity of the patient was less than 3% of that of the control, which was confirmed by measuring his plasma collected after an interval of more than 1 month. The values were consistent with the data obtained by two other methods, a fluorogenic assay [10] and a chromogenic assay [11] (data not shown). As the assay of the ADAMTS13-activity inhibitors [1] showed no detectable inhibitors in the patient plasma (data not shown), the etiology of his TTP symptoms was considered a genetic deficiency of ADAMTS13, that is, USS. To clarify the underlying cause of the TTP crisis, we analyzed the nucleotide sequences of the family's *ADAMTS13* genes.

DNA experiments were carried out with the permission of the ethics committees of the National Cardiovascular Center after obtaining informed consent from the study subjects. The nucleotide sequences of all 29 exons of *ADAMTS13*, including the intron-exon boundaries, were determined by direct sequencing of polymerase chain reaction (PCR) products as described previously [12,13].

The patient was heterozygous for five nucleotide mutations, c.964T>G, c.968C>G, c.969C>A, c.970T>C and c.2723G>A. Of them, c.2723G>A was also detected in the father. The mother and sister were heterozygous for c.2708C>T, which was not found in the patient or his father (Fig. 1B).

The c.2723G>A mutation on exon 21 causing C908Y, heterozygously found in the patient and father, was previously reported by us as a causative mutation in another USS family [14]. This mutation causes the impaired secretion of ADAMTS13 [14]. The moderately decreased ADAMTS13 activity of the father in the present case could be explained by this single mutation. The c.2708C>T mutation on exon 21 causing S903L was heterozygously found in the mother and sister, whose plasma ADAMTS13 activities were normal. This suggested that S903L should not affect the ADAMTS13 activity. In fact, the allele frequency of S903L is 6.0% in the Japanese general population (our unpublished data), making it a common polymorphism.

Correspondence: Koichi Kokame, National Cardiovascular Center Research Institute, 5-7-1 Fujishirodai, Suita, Osaka 565-8565, Japan. Tel.: +81 6 6833 5012; fax: +81 6 6835 1176; e-mail: kame@ri.ncvc.go.jp

Received 29 October 2007, accepted 29 October 2007

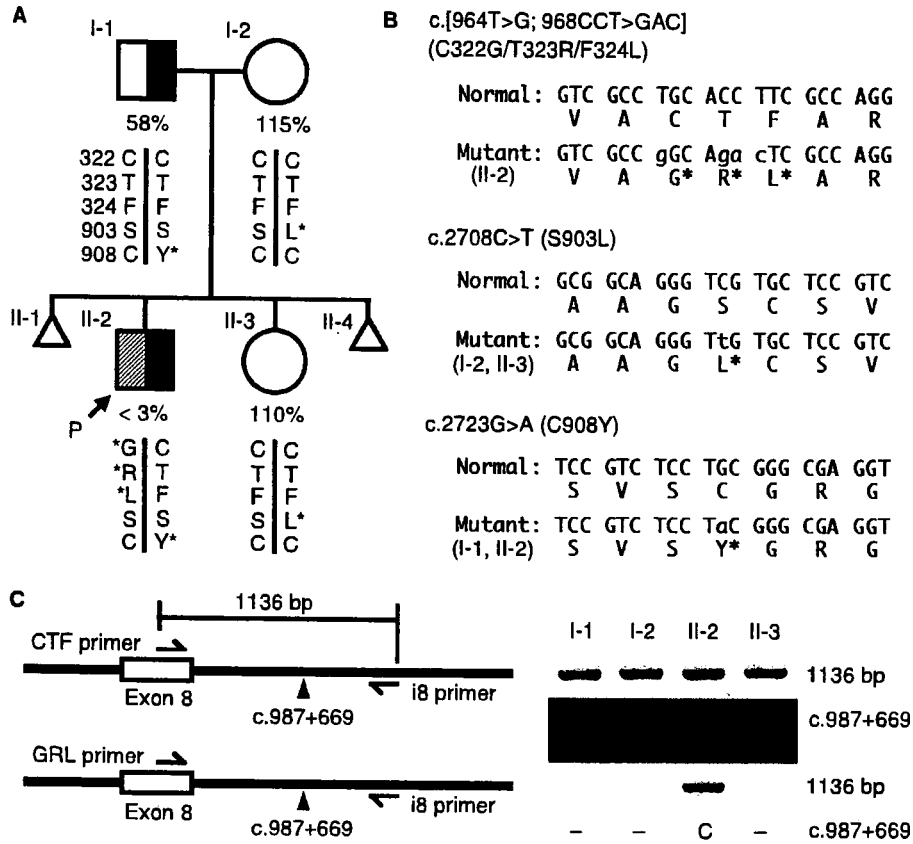


**Fig. 1.** *ADAMTS13* mutations in the USS patient *P* family. (A) Pedigree of the patient family. Plasma ADAMTS13 activities are shown under each symbol. The haplotype patterns of the five amino-acid residues deduced from each *ADAMTS13* gene are indicated under the ADAMTS13 activities. The arrow indicates the proband. (B) Missense mutations of *ADAMTS13* identified in this family. S903L is a common polymorphism. Asterisks indicate the mutated amino-acid residues. (C) PCR analysis of normal and mutant alleles. The 1,136-bp region was amplified by PCR using either the normal allele-specific CTF primer (5′-CCAAGGCTGTCGCCTGCACCT-3′) or the mutant allele-specific GRL primer (5′-CCAAGGCTGTCGCCGGCAGAC-3′) on exon 8 with the common reverse i8 primer (5′-TGAAGCCAGGAGTCCTAGACA-3′) on intron 8. This region contained a single nucleotide G/C polymorphism at the site of c.987 + 669. Subjects I-1 (father) and I-2 (mother) were homozygotes for G and C, respectively. The normal and mutant alleles of II-2 (patient) carried G and C, respectively.

The four mutations on exon 8, c.964T>G, c.968C>G, c.969C>A and c.970T>C, were detected only in the patient, suggesting that they should be *de novo* mutations in the patient's *ADAMTS13*. All the four mutations were excluded as common polymorphisms by the screening of 346 individuals in the Japanese general population. Cloning and sequencing of the genomic PCR products including exon 8 revealed that all the mutations were located on a single allele. Therefore, they could be described as c.[964T>G; 968CCT>GAC], resulting in three contiguous missense changes C322G/T323R/F324L within the disintegrin-like domain of ADAMTS13. The C322G mutation may disrupt a tertiary structure of the protein because of the defect in disulfide bond formation.

To determine the origin of the freshly mutated allele of the patient, a longer region including exon 8 was amplified by PCR using a combination of either the normal allele-specific CTF primer or the mutant allele-specific GRL primer and the common reverse i8 primer (Fig. 1C). The combinatorial use of CTF and i8 primers produced a 1,136-bp fragment from genomic DNAs of all the family members, whereas the use of GRL and i8 primers produced a 1,136-bp fragment only from the patient, as expected. The region contained a single nucleotide G/C polymorphism at the site of c.987 + 669. Sequencing of the fragments suggested that the father and mother were homozygotes for G and C, respectively, and that the sister was heterozygous. The normal and mutant alleles of the patient carried G and C, respectively. These results suggested that the mutant allele of the patient was derived from one of the maternal alleles. Based on all of the data, we concluded that the patient was a compound heterozygote of paternally transmitted C908Y and freshly mutated C322G/T323R/F324L on the maternal allele.

In conclusion, this is the first report of a case of compound heterozygosity of inherited and *de novo ADAMTS13* mutations resulting in USS.

## Acknowledgements

We thank Y. Nobe for technical assistance. This work was supported in part by the Program for Promotion of Fundamental Studies in Health Sciences of the National Institute of Biomedical Innovation (NIBIO) of Japan, grants-in-aid from

the Ministry of Health, Labor, and Welfare of Japan, and grants-in-aid from the Ministry of Education, Culture, Sports, Science, and Technology of Japan.

## Disclosure of Conflict of Interests

The authors have no conflict of interest.

## References

1 Kinoshita S, Yoshioka A, Park YD, Ishizashi H, Konno M, Funato M, Matsui T, Titani K, Yagi H, Matsumoto M, Fujimura Y. Upshaw-Schulman syndrome revisited: a concept of congenital thrombotic thrombocytopenic purpura. *Int J Hematol* 2001; **74**: 101–8.

2 Levy GG, Nichols WC, Lian EC, Foroud T, McClintick JN, McGee BM, Yang AY, Siemieniak DR, Stark KR, Gruppo R, Sarode R, Shurin SB, Chandrasekaran V, Stabler SP, Sabio H, Bouhassira EE, Upshaw JD Jr, Ginsburg D, Tsai HM. Mutations in a member of the *ADAMTS* gene family cause thrombotic thrombocytopenic purpura. *Nature* 2001; **413**: 488–94.

3 Fujimura Y, Matsumoto M, Yagi H, Yoshioka A, Matsui T, Titani K. Von Willebrand factor-cleaving protease and Upshaw-Schulman syndrome. *Int J Hematol* 2002; **75**: 25–34.

4 Kremer Hovinga JA, Studt JD, Lämmle B. The von Willebrand factor-cleaving protease (ADAMTS-13) and the diagnosis of thrombotic thrombocytopenic purpura (TTP). *Pathophysiol Haemost Thromb* 2003; **33**: 417–21.

5 Matsumoto M, Yagi H, Ishizashi H, Wada H, Fujimura Y. The Japanese experience with thrombotic thrombocytopenic purpura-hemolytic uremic syndrome. *Semin Hematol* 2004; **41**: 68–74.

6 Sadler JE, Moake JL, Miyata T, George JN. Recent advances in thrombotic thrombocytopenic purpura. *Hematology Am Soc Hematol Educ Program* 2004; 407–23.

7 Lämmle B, Kremer Hovinga JA, Alberio L. Thrombotic thrombocytopenic purpura. *J Thromb Haemost* 2005; **3**: 1663–75.

8 Miyata T, Kokame K, Banno F, Shin Y, Akiyama M. ADAMTS13 assays and ADAMTS13-deficient mice. *Curr Opin Hematol* 2007; **14**: 277–83.

9 Furlan M, Robles R, Lämmle B. Partial purification and characterization of a protease from human plasma cleaving von Willebrand factor to fragments produced by in vivo proteolysis. *Blood* 1996; **87**: 4223–34.

10 Kokame K, Nobe Y, Kokubo Y, Okayama A, Miyata T. FRETS-VWF73, a first fluorogenic substrate for ADAMTS13 assay. *Br J Haematol* 2005; **129**: 93–100.

11 Kato S, Matsumoto M, Matsuyama T, Isonishi A, Hiura H, Fujimura Y. Novel monoclonal antibody-based enzyme immunoassay for determining plasma levels of ADAMTS13 activity. *Transfusion* 2006; **46**: 1444–52.

12 Kokame K, Matsumoto M, Soejima K, Yagi H, Ishizashi H, Funato M, Tamai H, Konno M, Kamide K, Kawano Y, Miyata T, Fujimura Y. Mutations and common polymorphisms in *ADAMTS13* gene responsible for von Willebrand factor-cleaving protease activity. *Proc Natl Acad Sci U S A* 2002; **99**: 11902–7.

13 Kokame K, Miyata T. Genetic defects leading to hereditary thrombotic thrombocytopenic purpura. *Semin Hematol* 2004; **41**: 34–40.

14 Matsumoto M, Kokame K, Soejima K, Miura M, Hayashi S, Fujii Y, Iwai A, Ito E, Tsuji Y, Takeda-Shitaka M, Iwadate M, Umeyama H, Yagi H, Ishizashi H, Banno F, Nakagaki T, Miyata T, Fujimura Y. Molecular characterization of *ADAMTS13* gene mutations in Japanese patients with Upshaw-Schulman syndrome. *Blood* 2004; **103**: 1305–10.

Volume 56(2): 175–182, 2008
Journal of Histochemistry & Cytochemistry
http://www.jhc.org

ARTICLE

# Differential Expression Patterns of NDRG Family Proteins in the Central Nervous System

Tomohiko Okuda, Koichi Kokame, and Toshiyuki Miyata

National Cardiovascular Center Research Institute, Osaka, Japan

**SUMMARY** The N-myc downstream-regulated gene (NDRG) family consists of four proteins: NDRG1, NDRG2, NDRG3, and NDRG4 in mammals. NDRG1 has been thoroughly studied as an intracellular protein associated with stress response, cell growth, and differentiation. A nonsense mutation in the NDRG1 gene causes hereditary motor and sensory neuropathy, Charcot–Marie–Tooth disease type 4D. We previously generated *Ndrg1*-deficient mice and found that they exhibited peripheral nerve degeneration caused by severe demyelination, but that the complicated motor abilities were retained. These results implied that other NDRG family proteins may compensate for the NDRG1 deficiency in the central nervous system. In this study we raised specific antibodies against each member of the NDRG protein family and examined their cellular expression patterns in the mouse brain. In the cerebrum, NDRG1 and NDRG2 were localized in oligodendrocytes and astrocytes, respectively, whereas NDRG3 and NDRG4 were ubiquitous. In the cerebellum, NDRG1 and NDRG4 were localized in Purkinje cells and NDRG2 in Bergmann glial cells. NDRG3 was detected in the nuclei in most cells. These expression patterns demonstrated the cell type-specific and ubiquitous localization of the NDRG family proteins. Each NDRG may play a partially redundant role in specific cells in the brain. (J Histochem Cytochem 56:175–182, 2008)

**KEY WORDS**
NDRG1
NDRG2
NDRG3
NDRG4
brain
Charcot–Marie–Tooth disease
oligodendrocyte
astrocyte
immunohistochemistry

THE N-myc downstream-regulated gene (NDRG) family consists of four proteins: NDRG1, NDRG2, NDRG3, and NDRG4 in mammals. They are intracellular proteins of 340 to 394 amino acids and share 53 to 65% sequence identities to each other (Okuda and Kondoh 1999; Zhou et al. 2001; Qu et al. 2002). Among this family of proteins, NDRG1 has been thoroughly studied as an inducible protein by a number of stress and pathological conditions (Kovacevic and Richardson 2006). *NDRG1* was first identified as a stress stimuli-induced gene (Kokame et al. 1996; Zhou et al. 1998). It was also reported as a downregulated gene in tumors (van Belzen et al. 1997), regulated by p53 (Kurdistani et al. 1998; Stein et al. 2004), associated with the differentiation and malignant states of cancers (Piquemal et al. 1999; Xu et al. 1999; Guan et al. 2000; Bandyopadhyay et al. 2003), and regulated by *N-myc* (Shimono et al. 1999).

Correspondence to: Toshiyuki Miyata, PhD, National Cardiovascular Center Research Institute, 5-7-1 Fujishirodai, Suita, Osaka 565-8565, Japan. E-mail: miyata@ri.ncvc.go.jp

Received for publication July 24, 2007; accepted October 22, 2007 [DOI: 10.1369/jhc.7A7323.2007].

*NDRG1* is the gene responsible for Charcot–Marie–Tooth disease type 4D (CMT4D), also called hereditary motor and sensory neuropathy-Lom (Kalaydjieva et al. 1996,2000). Patients exhibit early-onset peripheral neuropathy, which progresses in adulthood to severe disability characterized by muscle weakness, sensory loss, and neural deafness. Diseases caused by deficiency of NDRG2, NDRG3, or NDRG4 have not yet been identified. Although studies about the NDRG family proteins have been accumulating, their molecular functions are still elusive.

To clarify the physiological roles of NDRG1, we generated *Ndrg1*-deficient mice and analyzed their phenotypes (Okuda et al. 2004). They exhibited a progressive demyelinating disorder of the peripheral nerves. Sporadic demyelination began by 5 weeks of age in the sciatic nerve, whereas the proliferation of Schwann cells and initial myelination were normal for 2 weeks after birth. In wild-type mice, NDRG1 was abundantly expressed in the cytoplasm of Schwann cells rather than in the myelin sheaths. Therefore, NDRG1 deficiency leads to autonomous dysfunction of Schwann cells, resulting in demyelination in peripheral nerves. This suggests that NDRG1 is essential for the maintenance of


0022-1554/07/$3.30

myelin sheaths in peripheral nerves. In contrast to muscle weakness caused by peripheral nerve degeneration, the complicated motor abilities in *Ndrg1*-deficient mice were relatively retained. These results suggest that functional compensation for NDRG1 deficiency may exist in the central nervous system (CNS).

Transcripts of NDRG1, NDRG2, NDRG3, and NDRG4 have been detected in the brain (Zhou et al. 2001; Okuda et al. 2004). In the present study we raised specific antibodies against each member of NDRGs and examined their expression patterns in the mouse CNS by immunohistochemical analysis. We found the cell type-specific and ubiquitous localization of NDRGs.

## Materials and Methods

### Animals

Adult male mice (C57BL/6 Cr Slc) aged 8 to 12 weeks (Japan SLC Inc.; Hamamatsu, Japan) were used in this study. Adult or 4-week-old *Ndrg1*-deficient male mice (Okuda et al. 2004) were also used. Mice were bred at a controlled temperature (22C) and lighting (lights on at 8 AM and off at 8 PM) for at least 1 week. Animal experiments were conducted in accordance with the guidelines for the care and use of experimental animals of the National Cardiovascular Center in Japan.

### Antibodies and Vectors

Rabbit polyclonal anti-human NDRG1 and anti-human NDRG4 antibodies were raised against bacterial recombinant glutathione S-transferase-fusion proteins of NDRG1 and NDRG4, respectively, and purified by the fusion protein-immobilized affinity column chromatography (Agarwala et al. 2000; Zhou et al. 2001). Rabbit polyclonal anti-NDRG2 and anti-NDRG3 antibodies were raised against the following synthetic peptides conjugated with keyhole limpet hemocyanin and purified by peptide-immobilized affinity column chromatography: $Q^{351}$SSESGTLPSGPPGH$^{365}$ for mouse NDRG2 and $F^{343}$SRSVTSNQSDGTQE$^{357}$ for mouse NDRG3. The mouse monoclonal anti-2′,3′-cyclic nucleotide 3′-phosphodiesterase (CNPase) antibody (clone 11-5B) was purchased from Sigma-Aldrich (St Louis, MO). Mouse monoclonal anti-glial fibrillary acidic protein (GFAP) antibody and mouse monoclonal anti-neuronal nuclei (NeuN) antibody were purchased from Chemicon (Temecula, CA).

Expression vectors for the green fluorescent protein (GFP)-fusion proteins of mouse NDRG1, NDRG2, NDRG3, and NDRG4 were constructed with the pEGFP-N1 vector (Clontech; Mountain View, CA). COS-1 cells were transfected with these vectors using the FuGENE6 transfection reagent (Roche Diagnostics; Indianapolis, IN). Two days later, cells were collected and lysed with lysis buffer (10 mM Tris–HCl, 2 mM EDTA, 50 mM dithiothreitol, 2% SDS, 6% glycerol, pH 6.8).

### Western Blotting Analysis

The excised whole brain was homogenized in the lysis buffer. Protein lysates were subjected to SDS-PAGE (10–20% gradient gel; Daiichi Pure Chemicals, Tokyo, Japan) and transferred to a polyvinylidene difluoride membrane (Bio-Rad; Hercules, CA). An equal amount of loading of the protein samples was confirmed by using the RC DC protein assay kit (Bio-Rad). After blocking with 3% skim milk in PBS with 0.05% Tween-20, the membrane was incubated with 0.5-μg/ml antibodies and then with a 1:1000 dilution of peroxidase-conjugated goat anti-rabbit IgG (Zymed; South San Francisco, CA). Chemiluminescent signals were developed using Western Lightning Chemiluminescence Reagent Plus (PerkinElmer Life Sciences; Wellesley, MA) and detected by an image analyzer LAS-1000plus (Fuji Film; Tokyo, Japan).

### Histological Analyses

Mice (8–12 weeks old) were anesthetized with Nembutal (Abbott Laboratories; North Chicago, IL) and perfused with ice-cold 4% paraformaldehyde in PBS. Brain was then excised and fixed in 4% paraformaldehyde in PBS overnight at 4C. For light microscopy, specimens were embedded in paraffin by standard procedures. Four-μm-thick paraffin sections were stained with hematoxylin–eosin or luxol–fast blue (Klüver-Barrera staining). Slides were examined with the Axioplan 2 microscope (Carl Zeiss; Oberkochen, Germany). For immunofluorescence microscopy, 4% paraformaldehyde-fixed brain specimens were washed with PBS at 4C, immersed in a 10–20% sucrose concentration ascending series in PBS overnight at 4C, and embedded in optimal cutting temperature compound (OCT; Sakura Finetek Torrance, CA) on dry ice. Five-μm-thick frozen sections were cut by a cryostat microtome and washed with PBS. After blocking with 10% normal goat serum for 30 min at room temperature, sections were incubated with a 1 μg/ml solution of each anti-NDRG antibody, a 1:200 dilution of anti-CNPase, a 1:200 dilution of anti-GFAP, and a 1:200 dilution of anti-NeuN overnight at 4C. They were then incubated with a 1:200 dilution of AlexaFluor 488-conjugated anti-rabbit IgG antibody and/or a 1:200 dilution of AlexaFluor 546-conjugated anti-mouse IgG antibody (Invitrogen; Carlsbad, CA) for 1 hr at room temperature. Fluorescence was detected with the Axiovert 200 microscope and photographed with the AxioCam (Carl Zeiss). For negative controls of immunostaining, normal rabbit IgG was used as a primary antibody instead of as a specific antibody.

## Results

### Raising Specific Antibodies Against the NDRG Family Proteins

We previously raised antibodies against human NDRG1 and NDRG4 (Agarwala et al. 2000; Zhou et al. 2001). Western blotting analysis showed that anti-NDRG1 and anti-NDRG4 specifically reacted with recombinant mouse NDRG1-GFP and NDRG4-GFP, respectively, and that anti-NDRG1 faintly cross-reacted with recombinant mouse NDRG3-GFP (Figure 1). In addition to these antibodies, in the present study we raised antibodies against mouse NDRG2 and NDRG3. They specifically reacted with recombinant mouse NDRG2-GFP and NDRG3-GFP, respectively, without any cross-reactions (Figure 1).

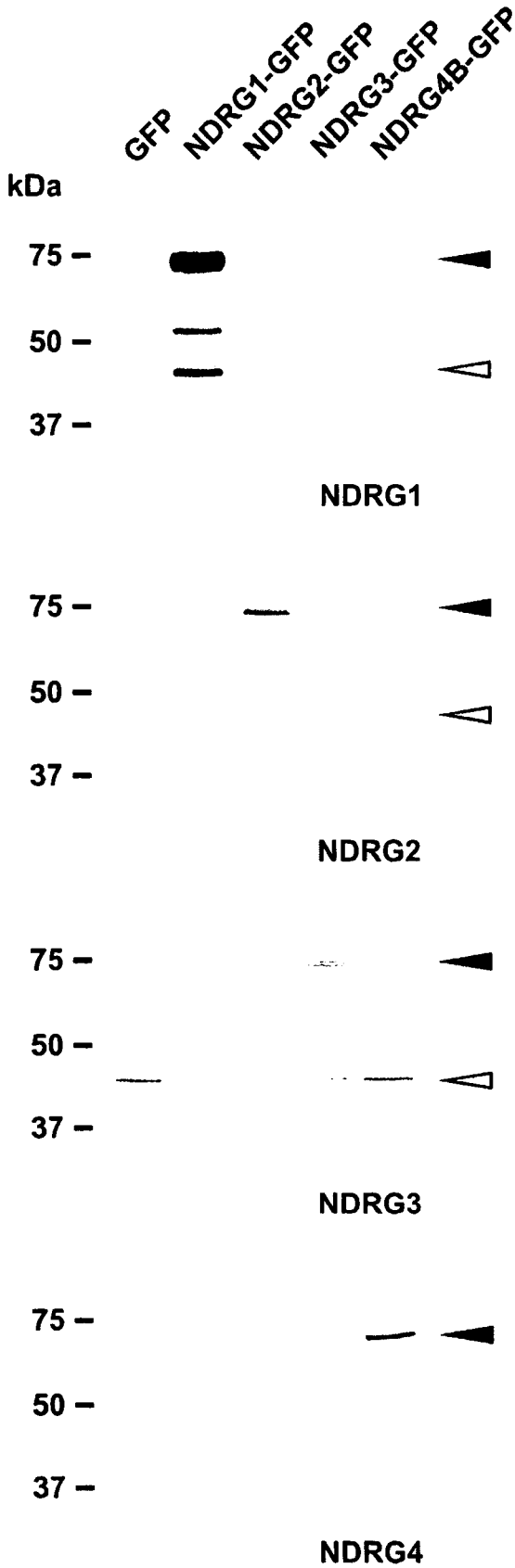


**Figure 1** Antibody specificity against NDRG family proteins. Lysates of COS-1 cells transfected with green fluorescent protein (GFP) or mouse NDRG–GFP vectors were analyzed by Western blotting. Each antibody specifically reacted with respective NDRG–GFP fusion proteins (closed arrowheads). Bands indicated by open arrowheads were endogenous NDRG proteins. Each lane contained 5 μg of total protein.

Using these antibodies, we detected all the NDRG family proteins in the brain of wild-type mice aged 4 and 12 weeks (Figure 2). Expression amounts of NDRG2, NDRG3, and NDRG4 proteins were not affected in the brain of *Ndrg1*-deficient mice, suggesting that the loss of NDRG1 did not affect expression levels of the other NDRGs (Figure 2).

### Histological Assessment of the Brain of *Ndrg1*-deficient Mice

We previously reported the phenotypes of *Ndrg1*-deficient mice (Okuda et al. 2004). They exhibited muscle weakness caused by peripheral nerve degeneration, but their complicated motor abilities were relatively retained. These phenotypes suggest that CNS can withstand the loss of NDRG1. According to the analysis of conventional histological sections,

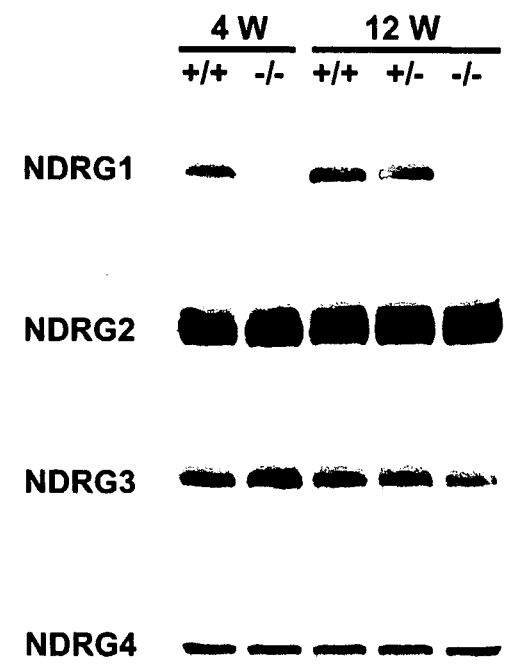


**Figure 2** Expression of NDRG family proteins in the mouse brain. Brain lysates were prepared from the wild-type and *Ndrg1*-deficient mice aged 4 or 12 weeks and analyzed by Western blotting. Each lane contained 5 μg of total protein. $^{+/+}$, wild-type mice; $^{-/-}$, homozygous *Ndrg1*-deficient mice; $^{+/-}$, heterozygous *Ndrg1*-deficient mice.

no abnormalities were observed in the brain of *Ndrg1*-deficient mice (Figure 3). Organization of the cerebral cortices and other laminated regions seemed normal (Figures 3A and 3B). The structure of the hippocampus in the *Ndrg1*-deficient mice was not different from the wild-type one (Figures 3C and 3D). Luxol–fast blue staining for the myelin sheaths revealed that myelination was not affected in the brain of *Ndrg1*-deficient mice (Figures 3E and 3F). Immunohistochemical analysis of the wild-type mouse brain using anti-NDRG1 antibody exhibited specific staining in the axon bundles of the corpus callosum, corpus striatum, and fimbria hippocampus (Figure 3G). These NDRG1-staining signals were not detected in the *Ndrg1*-deficient mouse brain (Figure 3H).

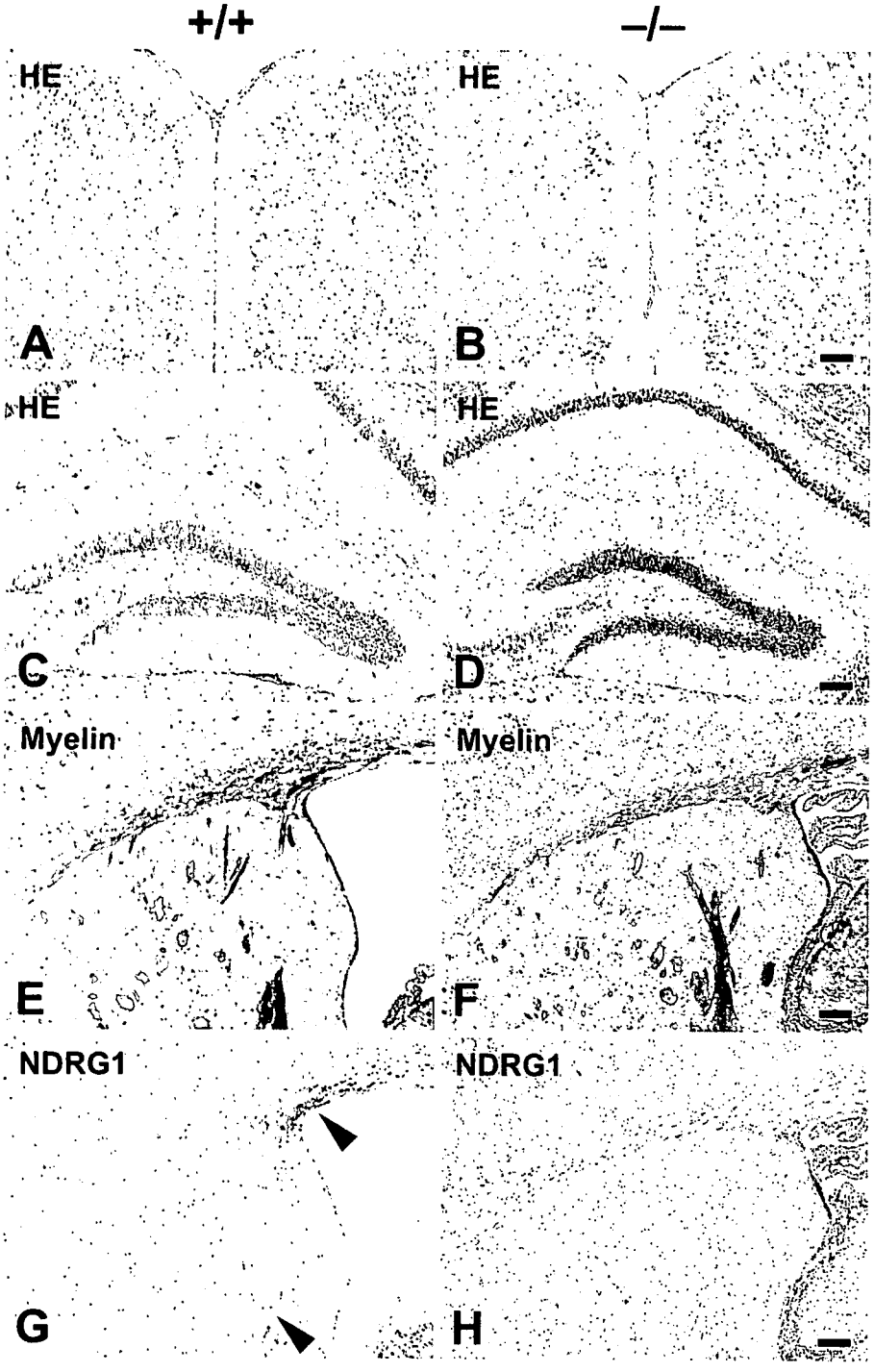


**Figure 3** Histological assessment of the brain of adult *Ndrg1*-deficient mice. Transverse sections of cerebral neocortex (**A,B**) and hippocampus (**C,D**) of adult wild-type ($^{+/+}$; **A,C**) and adult *Ndrg1*-deficient ($^{-/-}$; **B,D**) mice were compared. There were no significant differences in the structure of the brain regardless of genotype. Transverse sections of the forebrain at the level of the corpus callosum (**E,F**) and lateral ventricle (**G,H**) of adult wild-type (**E,G**) and adult *Ndrg1*-deficient (**F,H**) mice were compared. Normal myelination was observed in wild-type (**E**) and *Ndrg1*-deficient mice (**F**). NDRG1 was detected in the axon bundles of the corpus callosum and corpus striatum in wild-type mice (arrowheads in **G**). NDRG1 expression was not detected in the *Ndrg1*-deficient mice (**H**). HE, hematoxylin–eosin staining; myelin, luxol–fast blue staining; NDRG1, anti-NDRG1 immunostaining. Bar = 100 μm.

### Expression Patterns of NDRGs in the Brain

To investigate the expression characteristics of NDRGs in the brain, we performed immunohistochemical analysis using the antibodies specific for each NDRG. First, NDRG1 was strongly detected in the cytoplasm of oligodendrocytes in the cerebrum (Figure 4A). Specific expression of NDRG1 in the oligodendrocytes was confirmed by double staining for NDRG1 and CNPase. CNPase is a marker for oligodendrocytes (Figures 4C–4E). Although the cytoplasm was a principal site of NDRG1 localization, a fibrous staining pattern was also detected, suggesting that NDRG1 was partially localized in the processes of oligodendrocytes. In addition to the oligodendrocyte localization, weaker staining of NDRG1 was detected in Purkinje cells of the cerebellum (Figure 4B). NDRG1 was also strongly expressed in ependymal cells in the cerebrum (data not shown).

NDRG2 was strongly detected in the astrocytes of the cerebrum (Figure 5A), which was confirmed by double staining for NDRG2 and GFAP (Figures 5C–5E). GFAP is a commonly used marker for astrocytes. In the cerebellum, NDRG2 was also detected in Bergmann glial cells (Figure 5B). In both the cerebrum and cerebellum, NDRG2 was moderately expressed in most cells except neurons in the cerebral cortex and in Purkinje cells in the cerebellum (Figures 5A and 5B). Double staining for NDRG2 and NeuN indicated that NeuN-positive cells were NDRG2 negative in the cerebrum (Figures 5F–5H). NeuN is a marker for neurons. NDRG2 was less expressed in oligodendrocytes (data not shown). In the presence of immunogen peptides, anti-NDRG2 antibody did not give any signals (data not shown).

In contrast to the cytoplasmic localization of NDRG1 and NDRG2, expression of NDRG3 was observed in the nuclei of most cells in the cerebrum (Figure 6A). Nuclear localization of NDRG3 was also observed in other tissues (data not shown). Expression of NDRG3 was relatively strong in the neurons because most of the strong NDRG3-positive cells were NeuN-positive neurons (Figures 6C–6E). Significant expression of NDRG3 was also seen in the nuclei of Purkinje cells in the cerebellum, with less expression in the granule cells (Figure 6B). In the presence of immunogen peptides, anti-NDRG3 antibody did not give any signals (data not shown).

Expression of NDRG4 was detected in most brain cells, especially in the neurons of the cerebrum (Figure 7A, arrowhead) and Purkinje cells of the cerebellum (Figure 7B, open arrowhead). NDRG4-positive cells corresponded to cells expressing a neuron marker NeuN (Figures 7C–7E). NDRG4 was dominantly localized in the cytoplasm of these cells. Cytoplasmic localization of NDRG4 in Purkinje cells (Figure 7B) was similar to that of NDRG1 (Figure 4B). NDRG4 was less expressed in granule cells (Figure 7B) like NDRG1 (Figure 4B).

## Discussion

Although NDRG1 is essential for structural and functional maintenance of myelin sheaths in the peripheral nervous system (PNS) (Okuda et al. 2004), the morphology of the brain was not affected by the loss of NDRG1 (Figure 3). To understand the tissue- and cell-specific roles of NDRGs, the localization of each NDRG should be clarified in detail. In the present study we developed specific antibodies and examined

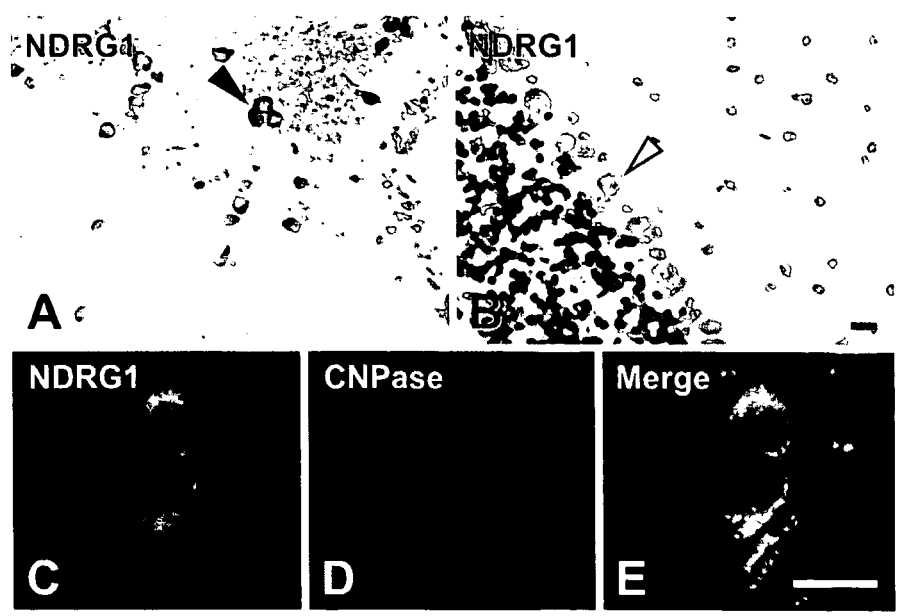


**Figure 4** Localization of NDRG1 in the brain. NDRG1 was detected in the cytoplasm of the oligodendrocyte in the cerebrum (arrowhead in A) and in Purkinje cells in the cerebellum (open arrowhead in B). Expression of NDRG1 (C) was colocalized with an oligodendrocyte-specific marker CNPase (D). Merged image is shown in E. Bar = 10 μm.